Geobiology of the Late Paleoproterozoic Duck Creek Formation, Western Australia

Citation

Published Version

Permanent link

Terms of Use

Share Your Story

Accessibility

2

3

4 Geobiology of the Late Paleoproterozoic Duck Creek Formation, Western

5 Australia

6

7

8 Jonathan P. Wilson[1,2*], Woodward W. Fischer[2], David T. Johnston[1], Andrew H. Knoll[3],

9 John P. Grotzinger[2], Malcolm R. Walter[5], Neal J. McNaughton[9], Mel Simon[4], John

10 Abelson[4], Daniel P. Schrag[1], Roger Summons[6], Abigail Allwood[7], Miriam Andres[8],

11 Crystal Gammon[2], Jessica Garvin, Sky Rashby[2], Maia Schweizer[2], Wesley A. Watters[6]

12

13

14 ABSTRACT

15 _____

16 The ca. 1.8 Ga Duck Creek Formation, Western Australia, preserves 1000 m of

17 carbonates and minor iron formation that accumulated along a late Paleoproterozoic

18 ocean margin. Two upward-deepening stratigraphic packages are preserved, each

19 characterized by peritidal precipitates at the base and iron formation and carbonate

20 turbidites in its upper part. Consistent with recent studies of Neoarchean basins, carbon

21 isotope ratios of Duck Creek carbonates show no evidence for a strong isotopic depth

22 gradient, but carbonate minerals in iron formations can be markedly depleted in ^{13}C. In

23 contrast, oxygen isotopes covary strongly with depth; δ^{18}O values as positive as 2‰

24 VPDB in peritidal facies systematically decline to values of -6 to -16‰ in basinal rocks,

* Corresponding author: jpwilson@caltech.edu
[1] Department of Earth and Planetary Sciences, Harvard University
[2] Division of Geological and Planetary Sciences, California Institute of Technology, Pasadena, CA USA
[3] Department of Organismic and Evolutionary Biology, Harvard University
[4] The Agouron Institute
[5] Australian Centre for Astrobiology, University of New South Wales, Australia
[6] Massachusetts Institute of Technology
[7] Jet Propulsion Laboratory
[8] Chevron Corp.
[9] Curtin University of Technology, Australia

1 reflecting, we posit, the timing of diagenetic closure. The Duck Creek Formation

2 contains microfossils similar to those of the Gunflint Formation, Canada; they are

3 restricted to early diagenetic cherts developed in basinal facies, strengthening the

4 hypothesis that such fossils capture communities driven by iron metabolism. Indeed, X-

5 ray diffraction data indicate that the Duck Creek basin was ferruginous throughout its

6 history. The persistence of ferruginous waters and iron formation deposition in Western

7 Australia for at least several tens of millions of years after the transition to sulfidic

8 conditions in Laurentia suggests that the late Paleoproterozoic expansion of sulfidic

9 subsurface waters was globally asynchronous.

10

11

13

1. Introduction

When the Paleoproterozoic Era (2500-1600 million years ago; Ma) began, Earth's biosphere contained little free oxygen (Holland, 2006). By the time it ended, however, sulfidic water masses commonly lay beneath an oxygenated atmosphere and surface ocean (Canfield, 1998; Shen et al., 2002, 2003; Brocks et al., 2005; Scott et al., 2008). Accumulating evidence suggests that Paleoproterozoic environmental transition was episodic, with an initial influx of O_2 near the beginning of the interval followed nearer to its end by a resurgence of iron formation and subsequent long term loss of ferruginous deep waters (Poulton et al., 2004, Johnston et al. 2006). Available paleobiological data are consistent with hypothesized environmental changes. For example, distinctive microfossil assemblages of the type first reported from cherts of the Gunflint Formation, Canada (Barghoorn and Tyler, 1965, Cloud 1965), occur broadly in successions deposited after the initial rise of atmospheric oxygen and before the long term loss of ferruginous deep waters. To date, however, there have been only limited attempts to integrate paleobiological, biogeochemical, and environmental geochemical data within a tightly constrained framework of sequence stratigraphy and geochronology.

To better understand the relationship between evolving ocean chemistry and Paleoproterozoic life, we examined the Duck Creek Formation, a late Paleoproterozoic carbonate platform preserved in the Ashburton Basin of Western Australia. The Duck Creek succession contains more than 1000m of well preserved carbonate-dominated stratigraphy. Early mapping (e.g., Daniels, 1970) facilitated reconnaissance level studies of microfossils (Knoll and Barghoorn, 1976; Schopf, 1983; Knoll et al., 1988) and carbon isotopes (Schopf, 1983; Veizer et al., 1992a; Lindsay and Brasier, 2002), as well as detailed investigations of stromatolites (Walter 1972; Grey 1985; Grey and Thorne, 1985) and sequence stratigraphy (Thorne, 1983; Grey and Thorne, 1985) through at least part of the succession. Moreover, SHRIMP U-Pb dates for zircons in intercalated volcanic rocks now constrain depositional ages for Duck Creek and succeeding Ashburton strata (see below). This study documents sequence development for the entire Duck Creek succession and uses this framework to interpret carbon and oxygen isotopes at high

1 stratigraphic resolution, in addition to mineralogical and paleobiological data from the

2 same samples.

3

4 **2. Geologic Setting**

5

6 In the northwestern corner of Western Australia, Paleoproterozoic sediments are

7 preserved in the Ashburton Basin, a 12 km package of siliciclastics, carbonates,

8 volcanics, and iron formation distributed over 30,000 km^2 (Figure 1). Accommodation

9 space resulted from crustal loading associated with collision of the Pilbara and Yilgarn

10 cratons during the Capricorn Orogeny, creating the Ashburton foreland (Thorne and

11 Seymour, 1991). The Paleoproterozoic Wyloo Group lies disconformably above

12 modestly to moderately metamorphosed iron formations, carbonates and other lithologies

13 of the Neoarchean-Paleoproterozoic Mount Bruce Supergroup. The Wyloo Group

14 contains two carbonate platforms capped by volcanics and a thick siliciclastic succession,

15 and was itself deformed during subsequent Capricorn events, with the metamorphic grade

16 increasing toward the south. Because deformation is basically limited to thin-skinned

17 folding and thrusting, the degree of structural rotation is, in most places, low (30-40°),

18 and overlying Ashburton Formation mudstones and iron formation have experienced only

19 sub-greenschist metamorphism. This is in contrast with the rocks of the Earaheedy

20 Group to the southeast, deposited on the southern margin of the orogen (Halilovic et al.,

21 2004; Jones et al., 2000).

22 Though clearly present throughout the fold-and-thrust belt (and visible from air

23 and satellite photos), outcrops of the middle Wyloo Group, including siliciclastic and

24 carbonate sediments of the Mount McGrath Formation and Duck Creek Dolomite, are

25 discontinuously exposed. However, just north of Wyloo Dome in the heart of the Duck

26 Creek Syncline, Duck Creek Gorge offers near continuous exposure of the Duck Creek

27 Formation on both sides of the drainage; this is the location of data presented here. Near

28 Paraburdoo, farther to the southeast along the outcrop belt, another nearly complete Duck

29 Creek Formation section is exposed. The formation is thinner there and appears to

30 contain a slightly different facies succession (Thorne 1983).

1   At Duck Creek Gorge (22°29'00"S, 116°19'10"E), carbonates cover a 4.5 km

2 transect as exposed in map view; over approximately half of that distance, vegetation and

3 alluvium prevent identification of bedrock (Figure 1). Within the gorge, basal Duck

4 Creek dolomites lie conformably above siltstones of the Mount McGrath Formation. To

5 the north of Duck Creek Gorge, the Duck Creek succession is overlain conformably by

6 basalt and tuffs of the June Hill Volcanics, whereas the southwestern portion of the

7 dolomite in the core of the Duck Creek Syncline is capped by the highly cleaved and

8 foliated fine-grained siliciclastics and iron formation of the Ashburton Formation. The

9 onset of Duck Creek sedimentation is constrained by a 2209±15 Ma SHRIMP U-Pb date

10 on the Cheela Springs Basalt, found lower in the Wyloo succession (Martin et al., 1998).

11 Its end is constrained by a series of ca. 1800 Ma SHRIMP U-Pb ages on June Hill

12 volcanic rocks, including a new U-Pb SHRIMP date on a tuff approximately 5km

13 northwest of the study site, reported here (Nelson, 2003; Sircombe, 2003; Evans et al.,

14 2003; see below). From the points of view of sedimentary patterns and basin analysis,

15 the age of the Duck Creek Formation lies relatively close to the minimum age constraint

16 provided by overlying June Hill tuffs (discussed below).

17

18 **3. Methods**

19

20   Rock samples were sectioned using a diamond saw and micro-drilled following

21 methods of Kaufman (1990) to obtain fresh powders. Carbonate $\delta^{13}C$ and $\delta^{18}O$ values for

22 418 samples were measured concurrently on a VG Optima dual inlet mass spectrometer

23 fed by an Isocarb preparation device in the Harvard University Laboratory for

24 Geochemical Oceanography. Carbonate samples (~1 mg) were dissolved in a common

25 anhydrous phosphoric acid (H_3PO_4) bath kept at 90°C for 8 minutes. Carbon dioxide gas

26 was purified cryogenically and subsequently measured against an in-house reference gas

27 (CO_2). Analytical uncertainty was ±0.1‰ (sample:standard ratio of 8:1); results are

28 reported on a Vienna Pee Dee Belemnite scale.

29   Mineralogical composition was measured for 18 samples distributed throughout

30 the formation. Constituent minerals were characterized by X-ray diffraction (XRD) with

31 a Scintag, Inc. XDS 2000 diffractometer, using Cu Kα_1 radiation at 40 kV and 30 mA

1   according to methods described by Tosca et al. (2004). For all samples, data were

2   collected at 0.02º 2θ steps, between 5º and 65º 2θ. Peak matching of XRD patterns was

3   done using Crystallographica Search-Match®, an iterative phase identification program

4   used for multiphase powder diffraction patterns. Multiphase patterns were matched

5   against the Powder Diffraction File with restrictions on phase chemistry that limited

6   searches to minerals containing common rock-forming elements (H, C, O, Na, Mg, Al,

7   Si, P, S, Cl, K, Ca, Mn, or Fe). Phases with best fits were removed from the spectrum

8   and the search was iterated for less-abundant phases. Mineral abundances were

9   quantified using XRD data and the publicly available RockJock spreadsheet (maintained

10 by the USGS and available at ftp://brrcrftp.cr.usgs.gov/pub/ddeberl). RockJock matches

11 measured XRD peaks to a database of mineral XRD peaks in order to quantify percent

12 abundances. Measured peaks were matched against a database of 22 carbonates and

13 rock-forming minerals and 17 clay minerals. In order to identify any expandable clays

14 that may have been present, a sample of the clay fraction from mid-Duck Creek iron

15 formation was saturated in ethylene glycol.

16   Zircons were separated from a tuffaceous ash bed within the overlying June Hill

17 Volcanics (Figure 1C) using conventional heavy liquid and magnetic techniques followed

18 by hand-picking by MinSep Laboratories, and mounted in epoxy with the BR266 zircon

19 reference standard (206Pb/238U age of 559 Ma and 903 ppm U). The epoxy mount was

20 polished to expose grain cores in section, imaged using a scanning electron microscope

21 and gold coated prior to SHRIMP (sensitive high resolution ion microprobe) analysis.

22 The SHRIMP analytical procedures follow Compston et al. (1984) and Smith et al.

23 (1998).

24

25

26 **4. Duck Creek Sequence Stratigraphy**

27

28   Thorne (1983; see also Grey and Thorne, 1985) provided detailed

29 sedimentological and sequence stratigraphic interpretation of a 220 m section of the

30 lower Duck Creek Formation prominently exposed in a canyon wall at Duck Creek

31 Gorge. This work builds on that framework and extends it to cover the entire Duck

1 Creek stratigraphy. In addition to the peritidal to shallow subtidal facies recognized by

2 Thorne (1983), major developments of subtidal stromatolitic bioherms, mound-and-

3 channel systems, deeper-water limestones interbedded with dolomitic turbidites, and iron

4 formation are present. These observations allow definition of the full suite of system

5 tracts within the Duck Creek sequences, with the result that a broader range of paleowater

6 depths can be reconstructed.

7 The Duck Creek Formation contains one complete depositional sequence, and

8 parts of two others; the base of the formation is marked by the highstand of an underlying

9 sequence, and the top of the formation is marked by the transgressive system tract of an

10 overlying sequence. This formation-capping transgressive system tract defines the

11 terminal drowning of the Duck Creek carbonate platform. The Duck Creek sequences are

12 defined on the basis of a single measured section, shown in Figure 2.

13

14 4.1. Sequence 1

15

16 *Highstand System Tract [0-142 meters].* The lower part of the Duck Creek Formation

17 comprises the upper, shallowing part of a highstand system tract. Lithostratigraphically,

18 the highstand is first recorded by the conformable contact with the underlying Mount

19 McGrath Formation, exposed at the eastern edge of Duck Creek Gorge. Across this

20 contact, black, tabular-bedded (~10 cm beds) Mount McGrath siltstones grade upward

21 into a fine-grained, white siltstone, capped in turn by hummocky- and swaly-cross-

22 stratified dolomite. Within the dolomite, large-amplitude (>20 cm) symmetric ripples,

23 teepee structures, and imbricate flat-pebble conglomerates occur, along with late

24 diagenetic cherts. The lowermost 40m, from the Mount McGrath contact, is the only part

25 of the Duck Creek Formation that exhibits sedimentary structures other than

26 stromatolites.

27 The presence of hummocky cross-stratification (HCS), as well as sedimentary

28 structures that include rip-ups, wave ripples, teepee structures and imbricate flat-pebble

29 conglomerates, indicates a moderate- to high-energy outer shoreface environment. HCS

30 is commonly associated with deposition above storm wave base (Einsele, 2000).

31 Imbricate clasts are more characteristic of storm-dominated, shallow-water environments

near or within the intertidal zone. Overall, the lower 38 m (section G, Figure 2) is
interpreted as a shallow marine dolostone, punctuated by deepening (as recorded by
HCS) to storm wave base.

These shallow water dolostones grade upward into ~100 m of m-scale
parasequences characterized by imbricated flat-pebble conglomerates, teepee structures,
and mitten-shaped stromatolitic precipitates. These peritidal facies mark the top of the
highstand system tract. The boundary between Sequence 1 and Sequence 2 is not
associated with karst or other evidence of subaerial exposure. Consequently, it is likely
that subsidence rates were sufficiently high to prevent long-term exposure.

4.2 Sequence 2

Sequence 2 is the only identified stratigraphic sequence contained entirely within
the lithostratigraphically-defined Duck Creek Formation.

Transgressive System Tract [142-258m]. The transgressive system tract of Sequence 2 is
marked by grainstones that are intercalated with three m-scale bioherms (at 150-152 m,
163-164 m, and 232-238 m), composed of close-packed, columnar stromatolites. In plan
view, the bioherms consist of circular- to elliptical columns with regular mm-scale
laminae and well-defined intercolumnar spacing, usually 1.1 ± 0.2 cm. Mound-and-
channel facies are present, as well, at 212-224 m and 224-232 m in the measured section.
The channel fills contain thin lenses of wrinkled, low-relief (<2 cm), heavily silicified
stromatiform precipitates. Locally, stromatolite initiation is marked by tungussiform
shapes that grade upward into vertical columns (Figure 3D).

Maximum Flooding Interval [258-260m]. The uppermost bioherm is capped by a
thin iron formation at 258 m that represents a maximum flooding interval. This ~ 1m
thick bed is the lower of two iron formations identified within the Duck Creek Formation.
(A third iron formation unit occurs in overlying beds of the lower Ashburton Formation.)
Hematite grains and dark blue early diagenetic chert nodules containing rare detrital
pyrite grains occur in two discrete layers within the Fe-rich unit. Indeed, while late
diagenetic silica is widely distributed in Duck Creek carbonates, early diagenetic (pre-

1   compaction) chert nodules occur only in the deeper facies that also host iron formation.

2   Above the iron formation, ~10 cm thick beds of imbricate flat-pebble conglomerate occur

3   within fine- to coarsely-laminated beds. These beds alternate on the meter scale with

4   domal, silicified dolomite precipitates.

5   *Highstand System Tract [260 – 440m]:* This is the Duck Creek interval

6   investigated by Grey and Thorne (1985). The first ~ 200 m above the MFI iron formation

7   represent shallowing to peritidal water depths and the formation of repetitive, stacked

8   peritidal parasequences (Figures 3, 4). Here 1 to 1.5 m parasequences of shallow-water

9   carbonates initiate with stromatolites of low synoptic relief draped by dolomitic

10 laminites, with locally extensive development of sub-cm-scale microdigitate, precipitated

11 stromatolites. Within this interval, parasequences are commonly capped by beachrock

12 that records sea level shallowing to exposure. Precipitated stromatolites include domal

13 structures up to 0.5 m high, laterally-linked conical structures with 3-4 cm of synoptic

14 relief, and fan-shaped domes truncated by flat-pebble conglomerates. Precipitated

15 stromatolite paraesquences are topped by a massive dolomitic grainstone. No chert

16 nodules were found in association with the precipitate units, but diffuse, late diagenetic

17 silicification is extensive. Under polarized light, precipitates contain rhomboidal

18 dolomite crystals with minimal bed-to-bed variability, only trace amounts of organic

19 matter, and some iron staining. Lamination is visible in hand-samples, but not in thin

20 section.

21   In agreement with previous investigators (Thorne, 1983; Grey and Thorne, 1985;

22 Lindsay and Brasier, 2002), the repeated pattern of low relief stromatolites truncated by

23 beach rock is interpreted to record inter- to supratidal deposition along the margin of a

24 carbonate ramp. Grainstones are rare, but truncation surfaces that record subaerial

25 exposure are common. It is possible that the uppermost of these exposed, peritidal

26 parasequences represents the boundary between Sequence 2 and Sequence 3. Similar to

27 what was observed at the top of Sequence 1, this boundary is not marked by a single

28 complex exposure surface. Instead, it appears that accommodation was substantial

29 enough to allow deposition throughout this time interval, making the distinction between

30 highstand and lowstand systems tracts difficult without further study of parasequence

31 stacking trends.

1

2   4.3 Sequence 3

3

4   *Transgressive System Tract [440-640m].* The peritidal strata of the Sequence 2

5   Highstand are overlain by massive dolomitic grainstones interbedded with occasional <1

6   meter beds of columnar stromatolites. These grainstones constitute the transgressive

7   system tract of Sequence 3. The grainstones grade upward into a ~20 m thick

8   stromatolitic bioherm composed of columnar stromatolites with regular and well-defined

9   intercolumnar spacing. And, like the Sequence 2 bioherms, this biohermal unit is

10   succeeded by a gradual transition to iron formation marking the further flooding and

11   backstepping of the platform to greater water depths.

12

13   *Maximum Flooding Interval [640-660m].*   The Sequence 3 maximum flooding

14   interval is distinctive in containing a significant iron formation, approximately 20 m

15   thick. This iron formation unit contains abundant early diagenetic chert and carbonate

16   nodules, in contrast to the much thinner iron formation in the MFI of Sequence 2.

17   Carbonates containing increasing abundances of potassium feldspars and hematite grade

18   into thin-bedded to laminated iron formation containing carbonate- and silica-rich phases.

19   Buff-weathering carbonate-rich beds alternate with hematite-rich beds near the base of

20   the iron formation, but bedded carbonates decrease in abundance through the ironstone.

21   In thin section, carbonates within the iron formation unit consist mostly of iron-stained

22   ankerite euhedra. The iron formation grades upward into a more carbonate-rich, white-

23   to brown-weathering unit composed of subangular iron-stained quartz grains mixed with

24   rhombohedral carbonate crystals. This, in turn, is capped by a minor further development

25   of hematitic ironstone and buff-weathering dolomite, similar to those found below the

26   carbonate.

27   Unfortunately, the iron formation is followed by ~ 100 m of cover where Duck

28   Creek takes a jog along strike, possibly as the result of a fault (Fig. 1c, indicated by

29   dashed line). Where outcrop resumes, the strata consist of monotonous, buff-weathered,

30   thickly-laminated dolostones (rhythmites) with fossiliferous early diagenetic chert

31   nodules and soft-sediment deformation structures (most commonly dm-scale slumps and

1   convolute bedding). These facies contain well-developed interbeds of tabular-clast,

2   matrix-supported breccias. Breccia clasts are derived from facies equivalents of the

3   interbedded rhythmites. This facies association is classically known from deeper-water

4   carbonate slope environments (Grotzinger, 1986).

5   It is possible the Sequence 3 MFI iron formation is immediately overlain by

6   shallower-water carbonate facies (not exposed), thus forming a highstand to Sequence 3.

7   However, the simplest interpretation of the covered interval is that it represents

8   resumption of carbonate production on the Duck Creek platform, but with transport into

9   deeper water environments. In this case it could still be a highstand deposit – albeit a

10   depositionally downdip, deeper water facies. Regardless, this covered interval contains

11   the transition to deeper water facies marking the onset of terminal flooding and drowning

12   of the Duck Creek platform.

13   Above the iron formation is a 40 meter slumped interval captured in section F,

14   overlapping the intact stratigraphy captured in section C. This slumped unit has discrete

15   margins that can be traced around the outcrop. It contains convolute bedding, and

16   abundant breccia, composed of imbricate, tabular buff-weathering dolomitic clasts up to

17   20 cm thick, set in a dark, rust-weathering carbonate matrix. This coarser breccia deposit

18   is provisionally interpreted as a slump facies (Figure 5). Where preserved, bed

19   orientation is discordant to the regular strike of the beds in the principal section. In thin

20   section, lower beds of this unit contain abundant and localized iron staining. Given the

21   anomalous isotopic compositions found within the off-section breccia; this unit is

22   discussed in more detail below.

23   *[660-1000m]:* Continuing upward in our primary section (from 860 to 942 m),

24   ferruginous limestone rhythmites are interbedded with dolomitic turbidites, displaying

25   well-defined Bouma sequences (Figure 5). Dolomitic turbidites occur approximately

26   every nine meters. Limestones are heavily silicified and pervasively stylolitized, and

27   contain dolomite nodules that are oblate to bedding and exhibit differential compaction.

28   The limestones commonly contain stylolites, often marked by high concentrations of iron

29   minerals. In thin section, limestones contain calcite crystals with small amounts of

30   hematitic coating, but the majority of iron is concentrated within stylolites, suggesting

31   that the limestones contained substantial amounts of iron at the time of stylolite

1   development. The presence of rhythmites and dolomitic turbidites, together with the

2   absence of wave-influenced sedimentary structures, suggests deposition in an iron-rich

3   environment well below wave-base and punctuated by turbidity currents. Near the top of

4   the unit, two ~1 meter thick beds of black, highly cleaved siltstone presage a change in

5   sedimentary regime, and following another ~150 m of cover the iron-rich, highly cleaved

6   siltstones of the Ashburton Formation begin.

7   In summary, the 1000m Duck Creek Formation preserves a sequence stratigraphic

8   architecture similar to that of other late Paleoproterozoic carbonate platforms (e.g.,

9   Grotzinger, 1986, 1989; Grotzinger and James, 2000): multiple sequences that grade

10   upward from shallow subtidal grainstones and stromatolitic bioherms to peritidal

11   carbonates with conspicuous precipitated microdigitate stromatolites. Maximum

12   flooding intervals contain iron formation and other authigenic carbonate/silicate

13   precipitates (see below), and slope/basinal facies are marked by (dolo)micrite and

14   limestone rhythmites, rhythmite breccias, block breccias, and carbonate turbidites.

15   Based on the presence of turbidites and slump features distal to peri- to supratidal

16   precipitates, the overall platform architecture is that of a distally-steepened carbonate

17   ramp. The repetitive sequence architecture enables us to differentiate between

18   geochemical and paleobiological patterns that reflect environment and those recording

19   secular change in a late Paleoproterozoic ocean.

20

21   **4. Mineralogy and Geochemistry**

22

23   *4.1 Mineralogical clues to paleoenvironmental history*

24

25   The Duck Creek Formation has long been characterized as dolomitic, with almost

26   no development of siliciclastic lithologies. X-ray diffraction (XRD) data, however,

27   shows that many Duck Creek carbonates are distinctly more iron-rich than this would

28   suggest. In peritidal and shallow subtidal facies, sampled carbonates are predominantly

29   ferroan dolomite $[Fe,Mg(CO_3)_2]$ and Mg- and Mn-rich ankerite

30    $[Ca(Mg_{0.27},Fe_{0.66},Mn_{0.05})(CO_3)_2]$ (Figure 3, Table 1), with lesser amounts (<10%) of

31   dolomite, quartz (as diffuse diagenetic silica), and, locally, clay minerals. Samples

1   associated with iron formation are distinctly different. Carbonate in these samples ranges

2   from a few to about 70% by weight, with dolomite, ankerite, and calcite in approximately

3   equal proportions. The iron formations contain up to 15% hematite and magnetite, as

4   well as chert (i.e. microcrystalline quartz) abundances much higher than those of other

5   facies. Clays and potassium feldspars, both authigenic, also reach their greatest

6   abundances in this facies. These potassium feldspars are probably diagenetic products of

7   preexisting zeolites and clays (Bish and Guthrie, 1993) based on their absence from hand

8   samples and petrographic thin sections. The lack of visible evidence for feldspars, but

9   their presence in XRD spectra, suggests that these minerals consist of small grains, which

10   would be expected from alteration of preexisting clay minerals. Deep water carbonates in

11   the upper part of the section differ again, consistently predominantly of calcite.

12   Silica and iron are closely correlated in Archean and Paleoproterozoic iron

13   formations (see Fischer and Knoll, 2009, for recent discussion), and in the Duck Creek

14   Formation, they covary on a sub-cm as well as outcrop scale. Throughout the formation,

15   siderite ($FeCO_3$) is present only in low abundances (<5%); this is not surprising given the

16   tendency of siderite to become dolomitized to ankerite (Klein and Beukes, 1989; Han

17   1978) or to decompose to magnetite (Fe_3O_4; Yui 1966) during burial diagenesis.

18   Although rare pyrite grains were observed in thin sections of early diagenetic chert

19   nodules, sulfide minerals are absent from bulk diffraction patterns throughout our sample

20   set.

21   Clay minerals occur as minor components of most samples, but comprise up to

22   20% of iron formation lithologies. Iron formation samples show XRD peaks at 6.4, 12.5,

23   and 26.6° 2θ, indicating the presence of chlorite, berthierine, and 1M illite, respectively

24   (Figure 3b). Glauconite is also found in lithologies associated with Duck Creek iron

25   formation, and, in a glycolated sample, a small break in slope at 2.54° suggests minor

26   occurrence of chaotically ordered expandable clay precursors, possibly smectite.

27   Berthierine [$(Fe,Al)_3(Si,Al)_2O_5(OH)_4$] and glauconite

28   [$K(Al,Fe,Mg)_2(Si,Al)_4O_{10}(OH)_2$] are particularly informative about Duck Creek

29   environments. These iron-rich, aluminum-poor clay minerals form in marine

30   environments at or near the sediment-water interface, in the presence of reduced iron and

31   commonly associated with organic matter. Glauconite precipitates slowly, commonly

1 under low rates of sedimentation which allow potassium to diffuse from the overlying

2 marine water column into its structure during formation (Meunier, 2005). Today,

3 glauconite typically forms below the thermocline, at water depths of 125 - 250m (10-

4 15°C). Berthierine typically occurs in nearshore settings associated with relatively warm

5 temperatures (for favorable precipitation kinetics), corresponding to 10-50m water depth

6 (25-27°C) in the modern ocean, above the thermocline.

7   The Duck Creek succession records this slight separation, as berthierine peaks at

8 ~642 meters, within the carbonate-rich ironstones, whereas glauconite peaks within the

9 iron formation at approximately 658 m and is present in the deeper water limestones.

10 Because both berthierine and glauconite form through redox reactions near the sediment-

11 water interface, rather than through metasomatism, they corroborate the evidence of Fe-

12 rich carbonates in indicating an iron-rich marine setting. 1M-illite in Duck Creek

13 samples probably reflects the digenetic transformation of original smectite clays.

14 Chlorite also occurs, but this mineral is typically the product of moderate metamorphism.

15   Heavily silicified samples from the lower part of the formation contain up to 7%

16 goethite. Like the possible smectite noted above, goethite in this section may have

17 originated relatively recently due to recent surface weathering. Goethite also provides a

18 fingerprint for zones of secondary alteration, and a possible indicator of areas where iron

19 minerals may be present due to present-day weathering elsewhere on the Pilbara Craton.

20 In the absence of core material, stratigraphic correlation between hematite and goethite

21 provides the most direct test of whether iron minerals formed from secondary alteration.

22 As noted above, hematite and other iron minerals reach their peak abundance within the

23 iron formation, rather than in the lower samples that have the highest concentrations of

24 goethite; this suggests at least some of the hematite in the iron formation is depositional.

25 That being said, it is clear from observations and hand samples that the entire

26 sedimentary sequence has been influenced by multiple episodes of diagenesis, most

27 obviously silicification.

28   In short, while iron formation provides the most obvious lithological

29 manifestation of ferruginous bottom-water conditions, both carbonate and clay

30 mineralogy indicate that the Duck Creek basin was iron-rich throughout the interval

31 recorded by our section. In coastal environments, continental run-off probably supplied

1   iron in oxidized form, which was reduced to Fe^{2+} within accumulating carbonates and

2   incorporated into Fe-dolomite and ankerite by dolomitizing fluids. Basinal iron

3   formations and associated Fe-carbonates more likely contain iron introduced from anoxic

4   deep waters.

5   That carbonates deposited during maximum flooding remain calcitic may

6   principally reflect the fact that basinal carbonates in the Duck Creek succession were

7   emplaced mechanically, transported from shallower sites of precipitation. Ferrous iron

8   would have been generated within anoxic deep waters and pore waters, but in the absence

9   of dolomitization -- known to be less prevalent in basinal environments (e.g., Grotzinger,

10   1989; Knoll and Swett, 1990) -- it was not readily incorporated into accumulating

11   carbonates.

12

13   *4.2 Carbon Isotopes*

14

15   High resolution carbon isotope data for the Duck Creek carbonates display a wide

16   range of variability, from -8.08 and +1.94‰, substantially greater than that reported by

17   earlier workers (Veizer et al., 1992b; Lindsay and Brasier, 2002). Despite the broad

18   overall range, however, a strong majority of measured values fall between +1.0 and -

19   0.5‰. The shallowest carbonates displaying precipitated textures exhibit the most

20   positive $\delta^{13}C$ values, averaging nearly 1‰, in contrast to subtidal stromatolites that

21   average 0‰. Similarly modest ^{13}C-enrichment of peritidal carbonates has previously

22   been recorded from Paleo- and Mesoproterozoic carbonates in other basins (e.g., Burdett

23   et al., 1990; Knoll et al., 1995; Hotinski et al., 2004). The Duck Creek succession

24   preserves carbonates deposited across a depth gradient likely to have exceeded 100 m,

25   but there is no further ^{13}C-depletion recorded in basinal limestones and dolomites. As

26   noted above, at least some deep water Duck Creek carbonates (breccias and turbidites)

27   reflect basinward transport of carbonates precipitated in shallower water. However, for

28   finer-grained facies this must be inferred.

29   That noted, the most negative $\delta^{13}C$ values in the Duck Creek succession do occur

30   in maximum flooding intervals within the succession, clustered into three sharp

31   excursions (Figure 2; see Table 1). Two of these are closely tied to the iron formations

1 developed in each major sequence; the third is contained within the megabreccia

2 appearing at 820-828 m in the upper part of the section (i.e. Section F).

3   A number of studies have reported large differences in carbonate carbon isotope

4 composition of shallow-water dolomitic carbonates (δ^{13}C ~0‰) and coeval carbonates

5 associated with basinal iron formation (δ^{13}C ~-5 to -7‰) (e.g., Becker and Clayton, 1972;

6 Beukes and Klein, 1990; Beukes et al., 1990; Kaufman et al., 1990). To explain this

7 gradient, conventional models invoke a stronger biological pump and a globally stratified

8 ocean capable of producing and maintaining a carbon isotope depth gradient (Derry et al.,

9 1992; Given and Lohmann, 1985; Hotinski et al., 2004; Kaufman et al., 1990; Kennedy,

10 1996; Surge et al., 1997). However, careful analysis of seafloor carbonate precipitates

11 deposited along a depth gradient in the late Paleoproterozoic Pethei Group, Canada,

12 detected no strong C-isotopic variation with depth (Hotinski et al., 2004). More recently,

13 detailed C-isotopic investigation of carbonates deposited along the margin of the

14 Neoarchean Campbellrand-Kuruman platform not only corroborated the absence of a

15 discernable C-isotopic depth gradient in seafloor precipitates formed across a paleodepth

16 range of several hundred meters, but also showed that siderites in basinal iron formation

17 differ from sub- and suprajacent $CaCO_3$ precipitates in recording variable, but commonly

18 strong ^{13}C-depletion (Fischer et al., 2009).

19   Such observations suggest that the ^{13}C depletion observed in iron formation

20 carbonates must reflect processes other than a hyperactive biological carbon pump.

21 Fischer et al. (2009) proposed that carbon isotope depletion associated with siderite, a

22 carbonate mineral often associated with iron formation, reflected complex interactions

23 among iron oxide minerals, soluble silica, and iron-reducing bacteria. In this model,

24 complexes of iron oxides and adsorbed silica were transported from surface waters to the

25 deep seafloor, where anaerobically respiring bacteria used the ferric iron as a terminal

26 electron acceptor. This resulted in the precipitation of mixed valence and reduced iron

27 minerals, including siderite.

28   Iron respiration is a heterotrophic process, oxidizing organic matter back to

29 carbon dioxide. Five analyses of organic carbon in Duck Creek carbonates yielded δ^{13}C

30 values of ca. -25‰; a single measurement of organic carbon in a Duck Creek chert

31 yielded a value of -31.7‰ (Schopf, 1983). Such fractionation is typical of ecosystems

1 fueled by RUBISCO-based autotrophy (House et al., 2000; Robinson and Cavanaugh,

2 1995). The depleted $\delta^{13}C$ signature from the oxidized or respired organics can contribute

3 to the dissolved inorganic carbon pool that feeds local precipitation of carbonate. Thus,

4 accumulating carbonates can contain markedly depleted $\delta^{13}C$ values, similar to those

5 observed in the Duck Creek Formation. Simple mass-balance would suggest that in the

6 most extreme of cases (-8‰; 658 m), 25-33% of the carbonate carbon came from

7 remineralized organic matter. The general expectation is that carbonates precipitated on

8 or within the seafloor in association with iron oxide minerals should record more

9 depleted $\delta^{13}C$ values than overlying or underlying iron oxide-poor facies. This is exactly

10 what is observed within the Duck Creek, and as such, provides a reasonable interpretation

11 for the lower two negative carbon isotope events.

12 As noted above, the uppermost negative carbon isotope anomaly is not associated

13 with iron formation. Carbonate minerals in this horizon are similar to those found in

14 shallow-water facies, comprising dolomite, ankerite, and Fe-dolomite. This unit contains

15 very little calcite and even less quartz, unlike other deeper-water samples above the iron

16 formation. Certain samples, however (specifically F0 and F6; Table 1), exhibit

17 significant iron staining on carbonate grains (Plate 3). This staining suggests that pore

18 fluid iron played a role in the diagenetic environment of these highly permeable breccias.

19 Percolating fluids could have supported a similar microbial iron-cycling community to

20 that found in association with the iron formation, resulting in a similar $\delta^{13}C$ signal.

21

22 *4.3. The $\delta^{18}O$ record*

23

24 Oxygen isotope ratios ($\delta^{18}O$) in ancient carbonates can provide a measure of post-

25 depositional water-rock interaction. Given that a vast majority of Precambrian

26 carbonates have been recrystallized, and secondary fluids are rich in O (from water), but

27 poor in C, the oxygen isotope composition of carbonates is differentially vulnerable to re-

28 setting. The result is that carbonates commonly acquire a $\delta^{18}O$ composition similar to

29 that of diagenetic waters, which commonly deviate from $\delta^{18}O$ composition of seawater

30 (Veizer et al., 1992a, 1992b). Although this classic interpretation has been challenged by

31 recent work exploring carbonate diagenesis through the lens of clumped isotope

1 paleothermometry, suggesting that diagnetic alteration can either enrich (via high-

2 temperature fluids) or deplete (via meteoric water) carbonates in ^{18}O (Came et al., 2007),

3 the simple claim that the $\delta^{18}O$ of carbonate is susceptible to alteration holds. This is our

4 point of entrance to the interpretation of Duck Creek $\delta^{18}O$ chemostratigraphy.

5         $\delta^{18}O$ values of the Duck Creek carbonates range from -14 to +5‰ VPDB (Figure

6 2). Perhaps surprisingly, O-isotopes show strong bathymetric coherence; shallow water

7 sections are relatively enriched in ^{18}O (~0 to 4‰; mean = 0.8‰), whereas deeper water

8 sections, including iron formation carbonates, are commonly more ^{18}O-depleted (mostly -

9 6 to +3‰; mean = -4.5‰). It has been suggested that a common mode of isotopic

10 behavior during diagemesis leads to covariation of carbon and oxygen isotope ratios

11 (Knauth and Kennedy 2009). In the Duck Creek Formation sections, $\delta^{13}C$ and $\delta^{18}O$

12 values do not covary, either through the section as a whole (Figure 8a) or within the

13 section at 600 to 700 meters, an interval marked by successive ^{13}C-depleted samples in

14 iron formation and ^{18}O-depletion in underlying carbonates (Figure 8b). The ^{18}O-depleted

15 carbonates contain carbon isotope values similar to shallow-water carbonates throughout

16 the section; ^{13}C-depleted ironstone samples contain oxygen isotope values similar to

17 intermediate to shallow carbonates throughout the section. The heaviest $\delta^{18}O$ values

18 recorded in our sample set occur in the megabreccia unit described earlier; comparable

19 $\delta^{18}O$ values have been interpreted as reflecting late-stage alteration by basinal fluids at

20 relatively elevated temperatures (50-70°C) (Came et al. 2007).

21   The pronounced stratigraphic pattern recorded by Duck Creek carbonates reflects

22 the relative timing of cementation, dolomitization and recrystallization processes that

23 collectively determine the extent to which sediments can interact with diagenetic fluids.

24 In peritidal environments, rapid cementation and penecontemporaneous dolomitization

25 commonly preserved least-altered stable isotopic signals (Burdett et al., 1990). In deeper

26 subtidal settings, however, cementation and dolomitization commonly occur later, if at

27 all, allowing calcium carbonate minerals to recrystallize in continuing contact with

28 diagenetic fluids depleted in ^{18}O (Burdett et al., 1990, Schidlowski et al., 1983,

29 Zempolich et al., 1988).

30   Like many Precambrian carbonates, petrographic examination of Duck Creek thin

31 sections suggests wholesale recrystallization. This is supported by the widely variable

1   oxygen isotope composition seen in the dataset. The stratigraphic pattern shows a

2   repeating monotonic trend through two deepening-upward cycles—specifically, small

3   first differences in $\delta^{18}O$ between stratigraphically contiguous samples. Shallow water

4   samples are typically enriched in ^{18}O (~2‰), whereas deep-water samples are ^{18}O-

5   depleted (-6‰). There is a general, but not one-to-one, correlation between percent

6   calcite and ^{18}O-enrichment, suggesting that oxygen isotope variation is controlled by the

7   vulnerability of calcite (compared to dolomite) to alteration during burial diagenesis.

8   Deeper-water sediments (e.g., limestones from sections D and E) have a higher

9   proportion of calcite and were cemented later (made clear from the differentially

10   compacted dolomite nodules in limestone matrix). Because mineralogy is a function of

11   depth, this gives the illusion of a depth gradient in oxygen isotope composition.

12

13   *4.4 Geochronology*

14   *Zircon morphology*: The morphology of zircons separated from sample JVT

15   includes typical tuffaceous sizes and shapes: i.e. 30-100 microns in size, aspect ratio

16   typically 1.5-2.0 with fine concentric euhedral internal zoning and euhedral to subhedral

17   external morphology. Several such grains show evidence of abrasion with chipped

18   external surfaces which crosscuts the internal euhedral zoning visible on

19   cathodoluminescence (CL) images. A minority of zircon grains are fragments of larger

20   grains, and also have the 30-100 micron size range and 1.5-2.0 aspect ratio.

21   *Age of the June Hill Volcanics*: The U-Pb isotopic data for the June Hill Tuff

22   sample are presented in Table 3. The 207Pb/206Pb age data shows considerable scatter

23   and reflects a complex zircon inventory in the tuffaceous sample. There is one dominant

24   age population (11 of 24 analyses <10% discordant) which comes exclusively from finely

25   zoned, euhedral to subhedral zircons typical of magmatic growth. All except one of these

26   analyses are ≤3% discordant (Table x) and they represent a single statistical age

27   population (MSWD = 0.84) which yields a pooled $^{207}Pb/^{206}Pb$ age of 1795+/-7 Ma (95%

28   c.l.; Fig. 11). This age is within analytical error of other estimates of the June Hill

29   Volcanics (discussed below) and given the zircon morphologies is considered to date the

30   tuffaceous event.

1   Other zircons in the sample are both older and younger. Five of the six older

2   zircons are within 1% of concordant and yield ages of 1834 to 3470 Ma (Appendix 3).

3   These grains are mostly fragments of larger grains with the external surface crosscutting

4   internal zonation in CL images. Most grains have rounded corners typical of detrital

5   grains and together with similar, although less severe, textures in the magmatic

6   population the tuff is interpreted to have been reworked. The age range of the older grains

7   corresponds to components of the underlying stratigraphy and granitoids and is

8   compatible with a hinterland of known Pilbara and Yilgarn Craton rocks at the time of

9   tuffaceous volcanism.

10   The younger grains found in the sample range in age from 1765 to 1185 Ma

11   (Appendix 3). All except one of these nine analyses are $\leq$2% discordant, which is unusual

12   if the normal explanations of diffusional Pb-loss and resetting are considered to explain

13   ages younger than the rock formation age. The three oldest grains of this group (i.e. 1742-

14   1765 Ma; Appendix 3) are morphologically similar to the 1795 Ma magmatic population

15   and are interpreted to be part of this group and suffered minor diffusional Pb-loss prior to

16   Recent times. Including these with the eleven magmatic analyses produces unexceptably

17   high scatter in the population for a single age (i.e. MSWD = 1.8 for n = 14) and validates

18   their omission from the magmatic group for the purposes of an age calculation.

19   The ages for the remaining six youngest analyses (Appendix 3) do not cluster to

20   indicate a discrete resetting event, and are mostly outside the age range of known events

21   to affect the rocks (e.g., the Capricorn Orogeny). Further, their shape and size are largely

22   indistinguishable from the other zircons in the rock. Although not definitive, this suggests

23   they were 1795 Ma or older zircon grains incorporated into the rock at its time of

24   formation and thereafter lost Pb by diffusion to fortuitously remain close to concordant.

25   Other explanations of partial resetting during unknown or poorly characterized events

26   after 1795 Ma remain possible but cannot be tested without more extensive studies,

27   which are outside the aim of determining the age of the tuffaceous volcanic event.

28

29   **5. Micropaleontology**

30

1   The modern era of Precambrian micropaleontology began with the discovery of

2   fossils in the ca. 1900 Ma Gunflint Formation, Canada (Tyler and Barghoorn, 1954;

3   Barghoorn and Tyler, 1965; Cloud 1965). Carbonaceous cherts associated with Gunflint

4   iron formation contain dense concentrations of microfossils, preserved as organic remains

5   or iron oxide replicas. Gunflint-like assemblages were subsequently recorded from other

6   late Paleoproterozoic iron formations, including the Sokomon Formation in Labrador,

7   Canada (Knoll and Simonson, 1981), and the Frere Formation, Australia (Walter et al.,

8   1976; Tobin, 1990). Gunflint-type assemblages differ markedly from the cyanobacterial

9   fossils found in silicified peritidal carbonates of comparable age from the Belcher

10   Islands, Canada (Hofmann, 1976; Golubic and Hofmann, 1976), suggesting that they may

11   record environmentally and/or metabolically distinct communities.

12   The sizes and shapes of Duck Creek microfossils are closely similar to those

13   found in Gunflint chert, including 1-2 µm filaments assigned to the genus *Gunflintia*,

14   small cocci assignable to *Huroniospora*, and asteriform microfossils placed within

15   *Eoastrion*, as well as rare larger trichomes comparable extant oscillatorian cyanobacteria

16   or sulfur-oxidizing bacteria (Knoll and Barghoorn, 1976; Knoll et al., 1988; Figure 9).

17   Microfossils in cherts collected within the measured section are similar to those reported

18   previously.

19   Early work on Duck Creek microfossil assemblages demonstrated their taxonomic

20   affinity to the Gunflint biota (Knoll and Barghoorn, 1976; Knoll et al., 1988) but lacked

21   the sequence stratigraphic context needed to facilitate environmental comparisons with

22   Canadian assemblages. Our stratigraphic investigation now provides a unique framework

23   to test the proposal (Knoll, 2003) that Gunflint-like biotas record iron-metabolizing

24   bacteria that lived close to the oxycline in ferruginous Paleoproterozoic oceans.

25   Early diagenetic silica provides an important taphonomic window on Proterozoic

26   life, and the processes that remove silica from seawater and redistribute it locally within

27   sediments to form nodules will strongly influence the types of communities seen through

28   this window. For much of Proterozoic time, silica left the oceans primarily as an early

29   stage evaporite, deposited along ocean margins (Maliva et al., 1989). For this reason,

30   peritidal mats rich in cyanobacteria are commonly found in early diagenetic cherts.

31   Adsorption on iron oxides, however, provides another means of removing silica from

1   seawater, and one that would have been important in Archean and Paleoproterozoic

2   basins where iron formation was deposited (Fischer and Knoll, 2009).

3   In the Duck Creek Formation, early diagenetic chert is essentially absent from

4   peritidal parts of the succession, but abundant in deeper facies associated with iron

5   formation. Not surprisingly, then, Duck Creek cherts contain no assemblages comparable

6   to that of the Belcher Islands, but abundant Gunflint-like fossils. Because peritidal

7   carbonates in the Duck Creek succession do not contain early diagenetic cherts, we

8   cannot be certain about microbial communities in that setting. That said, comparable

9   facies throughout the Proterozoic contain assemblages dominated by cyanobacteria and

10   cyanobacteria-like microfossils (Knoll 2003).

11   The presence of early diagenetic nodular cherts associated with iron deposition

12   suggests that the Duck Creek microbiota existed near (or slightly below) the sediment-

13   water interface, possibly close to a redoxcline. A redox interface would both provide a

14   chemical source of harvestable energy and ferrous iron for the iron formation. As early

15   as 1965, Cloud (1965) compared Gunflint filaments and asteriform microfossils with iron

16   bacteria found in modern ferruginous environments. Sequence stratigraphic

17   interpretation of Duck Creek microfossils supports such an interpretation and provides a

18   simple explanation for the apparent restriction of Gunflint-type assemblages to

19   Paleoproterozoic strata deposited after the initial rise of oxygen but before the demise of

20   Fe-rich deep waters (Knoll, 2003).

21

22   **6. Redox conditions in the Ashburton Basin**

23

24   More than a decade ago, Canfield (1998) proposed that the demise of

25   Paleoproterozoic iron formations resulted not from the expansion of oxygenated deep

26   waters but rather by the establishment of sulfidic chemistry in anoxic subsurface water

27   masses. In this hypothesis, the initial rise of oxygen in the atmosphere and surface ocean

28   resulted in an expanding sulfate reservoir. The presence of pyritic shales in latest

29   Paleoproterozoic rocks is hypothesized to represent an expansion of bacterial sulfate

30   reduction that resulted in the titration of ferrous iron from anoxic deep waters. The

31   global nature of redox conditions in late Paleoproterozoic deep waters remains uncertain,

1   although dysoxic, non-sulfidic water masses clearly existed (Slack et al., 2009). Water

2   masses immediately beneath the oxygenated mixed layer, however, were commonly

3   anoxic and sulfidic in latest Paleoproterozoic and Mesoproterozoic oceans (e.g., Shen et

4   al., 2002, 2003; Brocks et al., 2005; Scott et al., 2008).

5   In the late Paleoproterozoic Animike Basin of northwestern Ontario, hematitic

6   iron formation is overlain by sulfide-rich shales and siltstones. On the basis of Fe-

7   speciation studies, Poulton et al. (2004) proposed that this stratigraphic pattern captures

8   the transition from ferruginous to sulfidic subsurface waters, completed before ca. 1840

9   Ma. By itself, however, the Animike record cannot tell us (1) whether Paleoproterozoic

10   iron formations record the persistence or resurgence of Fe-rich deep waters, (2) whether

11   Paleoproterozoic ferruginous waters developed regionally or globally, or (3) whether the

12   transition to sulfidic subsurface waters occurred synchronously throughout the oceans.

13   Paleoproterozoic successions from Western Australia, including the Ashburton Basin,

14   provide perspective on these questions.

15   In Australia, iron formation occurs in a siliciclastic-dominated succession within

16   the Earaheedy Basin, on the conjugate side of the orogen associated with the Yilgarn

17   Craton (Halilovic et al., 2004). Commonly interpreted as correlative with Duck Creek

18   rocks, Earaheedy iron formation is constrained to be older than 1790-1760 Ma, the timing

19   of regional deformation (e.g., Halilovic et al., 2004). U-Pb SHRIMP dates on detrital

20   zircons in sandstones of the Yelma Formation deposited before the onset of iron

21   deposition indicate a depositional age younger than 1983 ± 51 Ma and 2032 ± 27 Ma;

22   detrital zircons in sandstones that overlie the iron formation include grains as young as

23   1808 ± 36 Ma (Halilovic et al., 2004).

24   As noted earlier, the age of the Duck Creek Dolomite is constrained U/Pb dates

25   on overlying June Hill Volcanics of 1806 ± 9 Ma (Nelson, 2003) and 1799 ± 8 Ma (Evans

26   et al., 2003). The new U-Pb date reported here is consistent with earlier determinations,

27   but is significant because the sampled ashbed lies directly on top of upper Duck Creek

28   Formation carbonates and below hematite iron formation of the overlying Ashburton

29   Formation in the same section (Thorne and Seymour, 1991). Thus, the 1795 ± 7Ma age

30   reported here provides direct confirmation that ferruginous waters persisted in the

1   Ashburton foreland basin until ca. 1800 Ma or later, a minimum of tens of millions of
2   years after they disappeared in North America.
3
4   **7. Conclusions**
5
6   The Paleoproterozoic Duck Creek carbonate platform developed in a basin
7   characterized by ferruginous bottom waters. Stromatolites in tidal flat to shallow subtidal
8   environments probably record benthic microbial communities fueled by cyanobacterial
9   photosynthesis (Grey, 1985). Deeper in the basin, however, an oxycline existed, with
10   moderately oxygenated waters above and anoxic ferruginous waters below. Near this
11   interface, iron metabolism played a major role in microbial ecosystems, with
12   chemotrophs and, possibly, phototrophs fixing carbon while iron-respiring bacteria
13   returned carbon dioxide to the environment. Gunflint-type microfossils preserved in
14   basinal Duck Creek cherts provide a fossil record of this community. The Duck Creek
15   Formation testifies to the presence of distinctive Proterozoic ecosystems whose
16   distribution in time and space waxed and waned with the distribution of iron-rich water
17   masses beneath oxic surface oceans.
18

25

References

Amard, B., Bertrand-Sarfati, J., 1997. Microfossils in 2000 Ma old cherty stromatolites of the Franceville Group, Gabon. Precambrian Research 81, 197-221.

Barghoorn, E.S., Tyler, S.A., 1965. Microorganisms from the Gunflint Chert. Science 147, 563-575.

Becker, R.H.,Clayton, R.N., 1972. Carbon isotopic evidence for the origin of a banded iron-formation in Western Australia. Geochimica et Cosmochimica Acta 36, 577-595.

Bekker, A., Kaufman, A.J., 2007. Oxidative forcing of global climate change: A biogeochemical record across the oldest Paleoproterozoic ice age in North America. Earth and Planetary Science Letters 258, 486-499.

Beukes, N.J., Klein, C., 1990. Geochemistry and sedimentology of a facies transition - from microbanded to granular iron-formation - in the Early Proterozoic Transvaal Supergroup, South-Africa. Precambrian Research, 47(1-2): 99-139.

Beukes, N.J., Klein, C., Kaufman, A.J. and Hayes, J.M., 1990. Carbonate Petrography, Kerogen distribution, and carbon and oxygen isotope variations in an Early Proterozoic transition from limestone to iron-formation deposition, Transvaal Supergroup, South-Africa. Economic Geology 85, 663-690.

Bish, D.L, Guthrie, G.D., 1993. Mineralogy of clay and zeolite dusts (exclusive of 1.1 layer silicates). Reviews in Mineralogy 28(1), 139-184.

Brocks, J.J., Love, G.D., Summons, R.E., Knoll, A.H., Logan, G.A., Bowden, S., 2005. Biomarker evidence for green and purple sulfur bacteria in an intensely stratified Paleoproterozoic ocean. Nature 437, 866-870.

Burdett, J.W., Grotzinger, J.P., and Arthur, M.A. 1990. Did major changes in the stable isotopic composition of Proterozoic seawater occur? Geology, v. 18, p. 227-230.

Came, R.E. et al., 2007. Coupling of surface temperatures and atmospheric CO2 concentrations during the Palaeozoic era. Nature 449, 198-201.

Canfield, D.E. 1998. A new model for Proterozoic ocean chemistry. Nature 396, 450-453.

Cloud, P.E., 1965. Significance of the Gunflint (Precambrian) microflora. Science 148, 28-35.

Compston, W., WIlliams, I. S., Meyer, C., 1984. U–Pb geochronology of zircons from lunar breccia 73217 using a sensitive high mass-resolution ion microprobe. Journal Geophysical Research, 89, B525–534.

Daniels, J.L., 1970. Explanatory notes:, Wyloo 1:250,000 geological sheet, Western Australia. Geological Survey of Western Australia, Perth, 20 p.

Derry, L.A., Kaufman, A.J., Jacobsen, S.B., 1992. Sedimentary cycling and environmental change in the Late Proterozoic: Evidence from stable and radiogenic isotopes. Geochimica et Cosmochimica Acta 56, 1317-1329.

Einsele, G., 2000. Sedimentary Basins: Evolution, Facies, and Sediment Budget. Springer-Verlag, Berlin.

Evans, D.A.D. et al., 2003. Revised geochronology of magmatism in the western
	Capricorn Orogen at 1805-1785 Ma: diachroneity of the Pilbara-Yilgarn collision.
	Australian Journal of Earth Sciences 50, 853-864.
Fischer, W.W., Knoll, A.H., 2009. An iron shuttle for deepwater silica in Late Archean
	and early Paleoproterozoic iron formation. Geological Society of America
	Bulletin 121, 222-235.

Fischer, W.W. et al., 2009. Isotopic constraints on the Late Archean carbon cycle from
the Transvaal Supergroup along the western margin of the Kaapvaal Craton, South
Africa. Precambrian Research, 169(1-4): 15-27.

Given, R.K., Lohmann, K.C., 1985. Derivation of the original isotopic composition of
	Permian marine cements. Journal of Sedimentary Research 55, 430-439.
Golubic, S., Hofmann, H.J., 1976. Comparison of Holocene and mid-Precambrian
	Entophysalidaceae (Cyanophyta) in stromatolitic algal mats: cell division and
	degradation. Journal of Paleontology 50, 1074-1082.
Grey, K., 1985. Stromatolites in the Duck Creek Dolomite, Western Australia.
	Geological Survey of Western Australia, Report 14, Professional Papers for 1983,
	pp. 94-103.
Grey, K.,Thorne, A.M., 1985. Biostratigraphic significance of stromatolites in upward
	shallowing sequences of the Early Proterozoic Duck Creek Dolomite, Western
	Australia. Precambrian Research 29, 183-206.
Grotzinger, J.P., 1986. cyclicity and paleoenvironmental dynamics: Rocknest platform,
	northwest Canada. Geological Society of America Bulletin 97, 1208-1231.
Grotzinger, J.P., 1989. Construction of early Proterozoic (1.9 Ga) barrier reef complex,
	Rocknest platform, Northwest Territories. Canadian Society of Petroleum
	Geologists Memoir 13, 30-37.
Grotzinger, J.P., James, N.P., 2000. Precambrian carbonates: evolution of understanding
	SEPM Special Publication 67, 3-20.
Halilovic, J., Cawood, P.A., Jones, J.A., Pirajno, F., Nemchin, A.A., 2004. Provenance of
	the Earaheedy Basin: implications for assembly of the Western Australian Craton.
	Precambrian Research 128, 343-366.

Han, T.-M., 1978, Microstructures of magnetite as guides to its origin in some
	Precambrian iron-formations: Fortschritte der Mineralogie, v. 56, p. 105–142.

Hofmann, H.J., 1976. Precambrian microflora, Belcher Islands, Canada; significance and
	systematics. Journal of Paleontology 50, 1040-1073.
Hofmann, H.J., Grotzinger, J.P., 1985. Shelf-facies microbiotas from the Odjick and
	Rocknest formations (Epworth Group; 1.89 Ga), northwestern Canada. Canadian
	Journal of Earth Sciences 22, 1781-1792.
Holland, H.D. 2006. The oxygenation of the atmosphere and oceans. Philosophical
	Transactions of the Royal Society, London, B-Bioloigcal Sciences 361, 903-915.
Hotinski, R.M., Kump, L.R., Arthur, M.A., 2004. The effectiveness of the
	Paleoproterozoic biological pump: A $\delta13C$ gradient from platform carbonates of

the Pethei Group (Great Slave Lake Supergroup, NWT). Geological Society of America Bulletin 116, 539-554.

House, C.H. et al., 2000. Carbon isotopic composition of individual Precambrian microfossils. Geology 28, 707-710.

Johnston, D.T. et al., 2006. Evolution of the oceanic sulfur cycle at the end of the Paleoproterozoic. Geochimica et Cosmochimica Acta, 70(23): 5723-5739.

Jones, J.A., Pirajno, F., Hocking, R.M., Grey, K., 2000. Revised stratigraphy for the Earaheedy Group: implications for the tectonic evolution and mineral potential of the Earaheedy Basin. Geological Survey of Western Australia Annual Review, 1999-2000, 57-64.

Kaufman, A.J., Hayes, J.M., Klein, C., 1990. Primary and diagenetic controls of isotopic compositions of iron-formation carbonates. Geochimica et Cosmochimica Acta 54, 3461-3473.

Kennedy, M.J., 1996. Stratigraphy, sedimentology, and isotopic geochemistry of Australian Neoproterozoic postglacial cap dolostones; deglaciation, $\delta^{13}C$ excursions, and carbonate precipitation. Journal of Sedimentary Research 66, 1050-1064.

Klein, C. and Beukes, N.J., 1989. Geochemistry and sedimentology of a facies transition from limestone to iron-formation deposition in the early Proterozoic Transvaal Supergroup, South Africa. Economic Geology, 84(7): 1733-1774.

Knauth, L.P. and Kennedy, M.J., 2009. The late Precambrian greening of the Earth. Nature, 460(7256): 728-732.

Knoll, A.H., 2003. Life on a Young Planet: The First Three Billion Years of Evolution on Earth. Princeton University Press, Princeton NJ.

Knoll, A.H. and Barghoorn, E.S., 1976. A Gunflint-type microbiota from the Duck Creek Dolomite, Western Australia. Origins of Life and Evolution of Biospheres 7, 417-423.

Knoll, A.H., Simonson, B. 1981. Early Proterozoic microfossils and penecontemporaneous quartz cementation in the Sokoman Iron Formation, Canada. Science 211, 478-480.

Knoll, A.H., Swett, K. 1990. Carbonate deposition during the late Proterozoic era: An example from Spitsbergen. American Journal of Science 290-A, 104-132.

Knoll, A.H., Kaufman, A.J., Semikhatov, M.A., 1995. The carbon-isotopic composition of Proterozoic carbonates - Riphean successions from northwestern Siberia (Anabar Massif, Turukhansk Uplift). American Journal of Science 295, 823-850.

Knoll, A.H., Strother, P.K., Rossi, S. 1988. Distribution and diagenesis of microfossils from the Lower Proterozoic Duck Creek Dolomite, Western Australia. Precambrian Research 38, 257-279.

Lindsay, J.F., Brasier, M.D., 2002. Did global tectonics drive early biosphere evolution? Carbon isotope record from 2.6 to 1.9 Ga carbonates of Western Australian basins. Precambrian Research 114, 1-34.

Maliva, R., Knoll, A.H., Siever, R. 1989. Secular change in chert distribution: a reflection of evolving biological participation in the silica cycle. Palaios 4, 519-532.

Martin, D.M., Li, Z.X., Nemchin, A.A., Powell, C.M., 1998. A pre-2.2 Ga age for giant hematite ores of the Hamersley province, Australia? Economic Geology 93, 1084-1090.

Martin, D.M., Powell, C.M., George, A.D., 2000. Stratigraphic architecture and evolution of the early Paleoproterozoic McGrath Trough, Western Australia. Precambrian Research 99, 33-64.

Meunier, A., 2005. Clays. Springer, Berlin, 472 pp.

Nelson, D.R., 2003. Compilation of SHRIMP U-Pb zircon geochronology data, 2002. Geological Survey of Western Australia Record, 2003(2).

Poulton, S.W., Fralick, P.W., Canfield, D.E., 2004. The transition to a sulphidic ocean ~1.84 billion years ago. Nature 431, 173-177.

Robinson, J.L., Cavanaugh, C.M., 1995. Rubisco in chemoautotrophic symbioses: Implications for the interpretation of stable carbon isotope values. Limnology and Oceanography 40, 1496-1502.

Schidlowski, M., Hayes, J.M., Kaplan, I.R., 1983. Isotopic inferences of ancient biochemistries: Carbon, sulfur, hydrogen, and nitrogen, in Schopf, J.W. (Ed.), Earth's Earliest Biosphere. Princeton University Press, Princeton NJ.

Schopf, J.W. (Ed.), 1983. Earth's Earliest Biosphere. Princeton University Press, Princeton NJ.

Scott, C., Lyons, T.W., Bekker, A., Shen, Y., Poulton, S.W. Chu, X., Anbar, A.D. 2008. Tracing the stepwise oxygenation of the Proterozoic ocean. Nature 452, 456-458.

Shen, Y.N., Canfield, D.E., Knoll, A.H. 2002. Middle Proterozoic ocean chemistry: Evidence from the McArthur Basin, northern Australia. American Journal of Science 302, 81-109.

Shen, Y., Knoll, A.H., Walter, M.R. 2003. Evidence for low sulphate and anoxia in a mid-Proterozoic marine basin. Nature 423, 632-635

Sircombe, K.N., 2003. Age of the Mt Boggola volcanic succession and further geochronological constraint on the Ashburton Basin, Western Australia. Australian Journal of Earth Sciences 50, 967-974.

Slack, J.F, Grenne, T., Bekker, A. 2009. Seafloor-hydrothermal Si-Fe-Mn exhalites in the Pecos greenstone belt, New Mexico, and the redox state of ca. 1720 Ma deep seawater. Geosphere 5(3), 302-314.

Smith, J.B. et al., 1998. The Sholl Shear Zone, west Pilbara: evidence for a domain boundary structure from integrated tectonostratigraphic analyses, SHRIMP U-Pb dating and isotopic and geochemical data of granitoids. Precambrian Research, 88(1-4): 143-171.

Surge, D.M., Savarese, M., Dodd, J.R., Lohmann, K.C., 1997. Carbon isotopic evidence for photosynthesis in Early Cambrian oceans. Geology 25, 503-506.

Thorne, A.M., 1983. Upward-shallowing sequences in the Precambrian duck Creek
    Dolomite, Western Australia. Western Australia Geological Survey Professional
    Papers 1985, 81-93.
Thorne, A.M., Seymour, D.B., 1991. Geology of the Ashburton Basin, Western Australia.
    Bulletin (Geological Survey of Western Australia). Geological Survey of Western
    Australia, Perth WA, 141 pp.
Tobin, K.J., 1990. The paleoecology and significance of the Gunflint-type microbial
    assemblages from the Frere Formation (Early Proterozoic), Nabberu Basin,
    Western Australia. Precambrian Research 47, 71-81.

Tosca, N.J., McLennan, S.M., Lindsley, D.H. and Schoonen, M.A.A., 2004. Acid-sulfate
weathering of synthetic Martian basalt: The acid fog model revisited. J. Geophys. Res.,
109.

Tyler, S.A., Barghoorn, E.S., 1954. Occurrence of structurally preserved plants in pre-
    Cambrian rocks of the Canadian Shield. Science 119, 606-608.
Veizer, J., Clayton, R.N. and Hinton, R.W., 1992a. Geochemistry of Precambrian
    carbonates: IV. Early Paleoproterozoic (2.25 ± 0.25 ga) seawater. Geochimica et
    Cosmochimica Acta 56, 875-885.
Veizer, J., Plumb, K.A., Clayton, R.N., Hinton, R.W. and Grotzinger, J.P., 1992b.
    Geochemistry of Precambrian carbonates: V. Late Paleoproterozoic seawater.
    Geochimica et Cosmochimica Acta 56, 2487-2501.
Walter, M.R., Goode, A.D.T., Hall, J.A., 1976. Microfossils from the newly discovered
    Precambrian stromatolitic iron formation in Western Australia. Nature 261,
    221–223.

Walter, M.R., 1972. Stromatolites and the biostratigraphy of the Australian Precambrian
    and Cambrian: Special Papers in Paleontology No. 11, 268 p.

Yui, S., 1966. Decomposition of siderite to magnetite at lower oxygen fugacities: a
    thermochemical interpretation and geological implications. Economic Geology
    61, 768-776.

Zempolich, W.G., Wilkinson, B.H., and Lohmann, K.C., 1988. Diagenesis of Late
    Proterozoic carbonates: The Beck Spring Dolomite of eastern California. Journal
    of Sedimentary Petrology 58, 656-672.

1
Figure Captions
3
Fig. 1. Tectonic map of Western Australia showing the location of the Capricorn Orogen
and related sedimentary basins. Map of Wyloo Group exposed at Duck Creek
Gorge, showing field relationship between units. Sections described in the text
are marked.

Fig. 2. Stratigraphy and C and O isotope ratio data. Three negative $\delta^{13}C$ excursions are
present. Oxygen isotope values ($\delta^{18}O$) follow deepening-upward sequences. Red
values indicate samples from section F, capturing a local slumped and brecciated
unit (see Plate 3). Sequence stratigraphic interpretations are shown: TST =
Transgressive System Tract, MFI = Maximum Flooding Interval, HST =
Highstand System Tract.

Fig. 3. (A) outcrop photo of Duck Creek Dolomite at Duck Creek Gorge, approximately
30 m of relief; (B) giant wave ripple, section G; (C) laminated precipitates
truncated by planar-bedded carbonates suggestive of intertidal environments,
section A; (D) mound-and-channel, section A; (E) iron formation, section A; (F)
peritidal precipitates draping needle-like crystal fans, section B.

Fig. 4. (A) Low-relief domal precipitates, section B; (B) conical precipitates, section B;
(C) early diagenetic chert nodule in iron formation, section C; (D) ironstone
within section C; (E) and calcite-rich carbonate within iron formation, section C.

Fig. 5. (A) Slumped and brecciated unit with iron-stained matrix, section F; (B) early
diagenetic and fossiliferous black chert, section C; (C) stylolitic limestones,
section D; (D) dolomitic turbidite in stylolitic limestone, section E; (E)
limestones, dolomitic turbidites, and siltstone unit at arrows, section E.

Fig. 6. Carbon isotope chemostratigraphy versus mineral abundances (determined by X-
ray diffraction abundances). Shallow-water sections contain iron-rich carbonates,
such as dolomite, ankerite, and Fe-dolomite (due to ferrous dolomitizing fluids).
Deep-water sections are dominated by iron-poor carbonates, such as calcite and
aragonite. Iron formations are rich in silica, iron, and clays. Potassium feldspars
peak in abundance within the iron formation. .

Fig. 7. X-ray diffraction trace, both glycolated and unglycolated, from a hematite-rich
iron formation sample, showing the presence of berthierine, illite, and chlorite.

Fig. 8. (A) Crossplot of $\delta^{13}C$ and $\delta^{18}O$ values from the complete section. (B)Crossplot
of $\delta^{13}C$ and $\delta^{18}O$ values from samples between 600 and 700 meters. Samples
which are depleted in ^{13}C are enriched in ^{18}O.

Fig. 9: (A) Chert 25 at 40x, showing *Eoastrion, Gunflintia, and Huroniospora*; (B) petrographic thin section of sample F0 at 40x showing iron staining on carbonate grains.

Fig. 10: Marine cross-section showing a summary of mid-Paleoproterozoic microfossil distributions. Previous Gunflint-type microbiotas occur in cherty stromatolites deposited in relatively shallow water (Amard and Bertrand-Safarti, 1997; Barghoorn and Tyler, 1965; Knoll and Simonson, 1981; Walter et al., 1976; Tobin, 1990), whereas fossiliferous cherts from from the Belcher Islands contain coccoidal cyanobacteria from the shallowest water depths (Hofmann, 1976; Golubic and Hofmann, 1976). The occurrence of a Gunflint-type assemblage in early diagenetic Duck Creek Formation cherts is useful because its stratigraphic context places Gunflint-type microfossils in an iron-rich deep water paleoenvironment. This relationship lends support to the proposed identification of these organisms as bacteria with iron-based metabolisms, as suggested by Cloud (1965).

Appendix 1: Oxygen and carbon isotope composition of samples.

Appendix 2: Stratigraphic distribution of minerals, based on X-ray diffraction analysis.

Appendix 3: U-Pb SHRIMP zircon data.

Pilbara Craton
Capricorn Orogen
Yilgarn Craton

115 22 117
Duck Creek syncline
Wyloo dome
Pilbara Craton
Hamersley Basin
Ashburton Basin
Bangemall Basin
24
Gascoyne Complex
Yilgarn Craton

116°18'50" E   22°29'00" S   116°19'00" E

22°29'30" S

116°18'50" E

Mt. Stuart Station

Ash bed

Duck Creek

A
B
C   G
32
F
Microfossils
D   Cover
E
70

Wyloo Dome

5 km

116°19'00" E   22°29'30" S

22°29'00" S
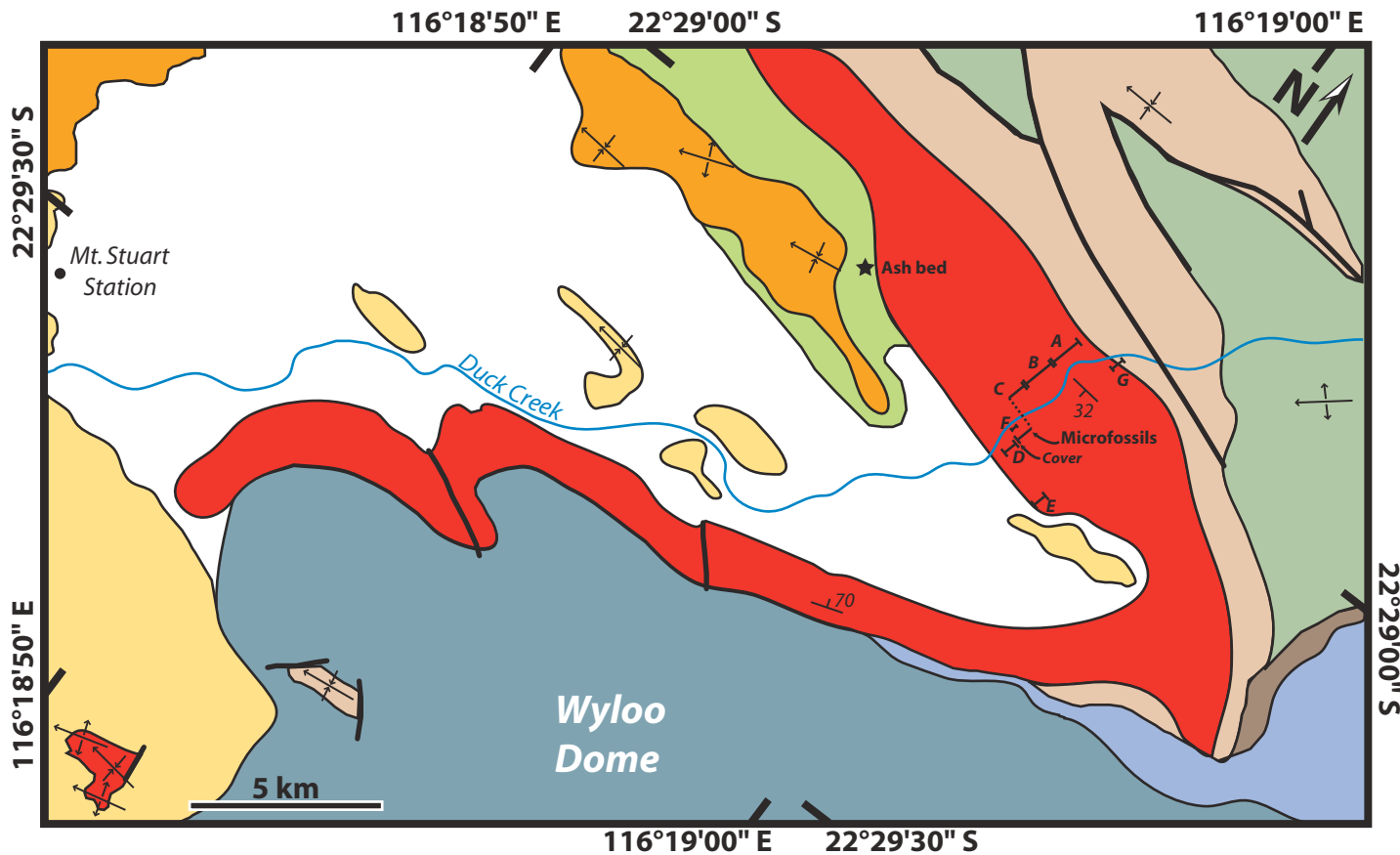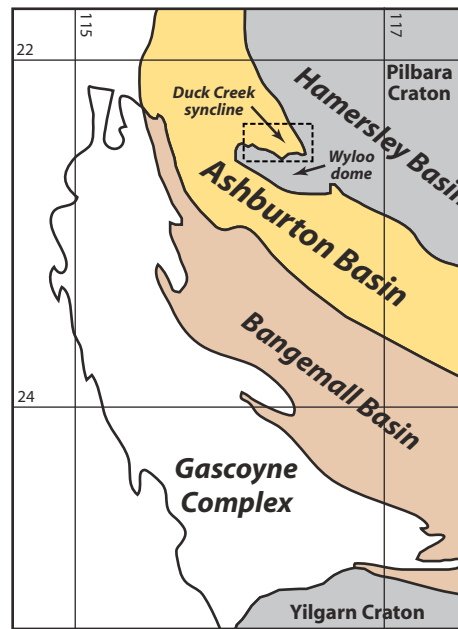
Duck Creek syncline stratigraphy

Cover and alluvium

Ashburton Formation & iron formation

June Hill Volcanics

Duck Creek Dolomite

Mount McGrath Formation

Cheela Springs Basalt

Beasley River Quartzite

Undifferentiated Hamersley Group

Undifferentiated Fortescue Group

Wyloo Group

O_2

$Fe(II)_{(aq)}$

Duck Creek microbiota
(Gunflint-type)

Cyanobacteria

June Hill Volcanics

1795 +/- 7 Ma
MSWD = 0.84
n = 11
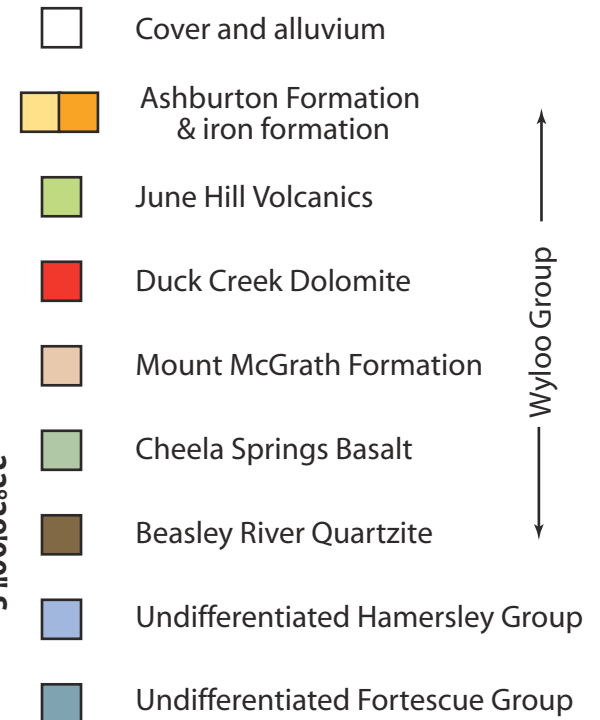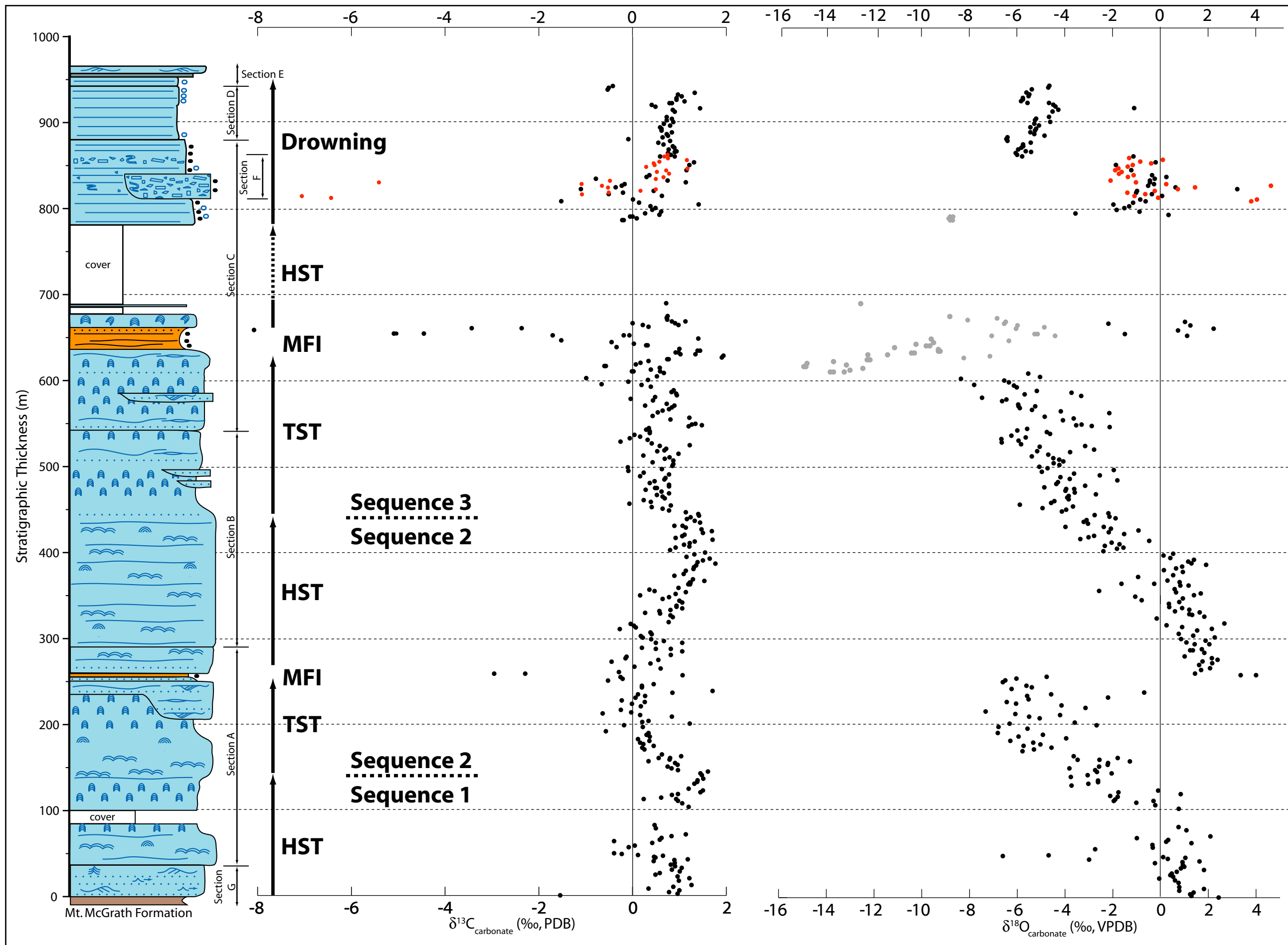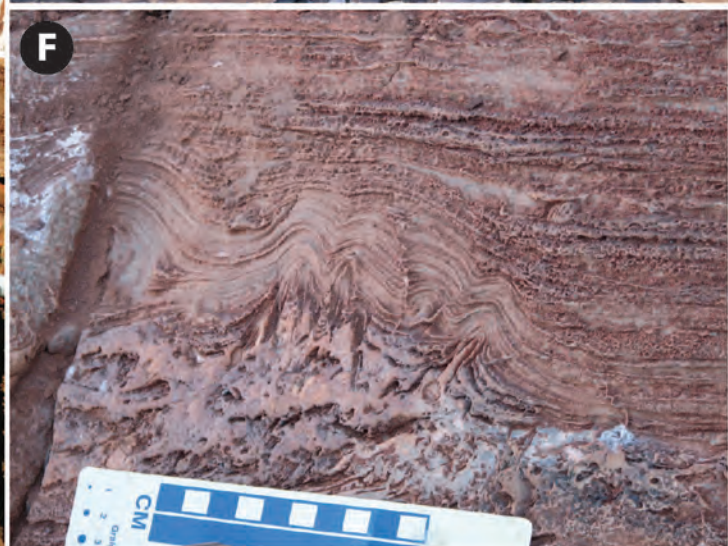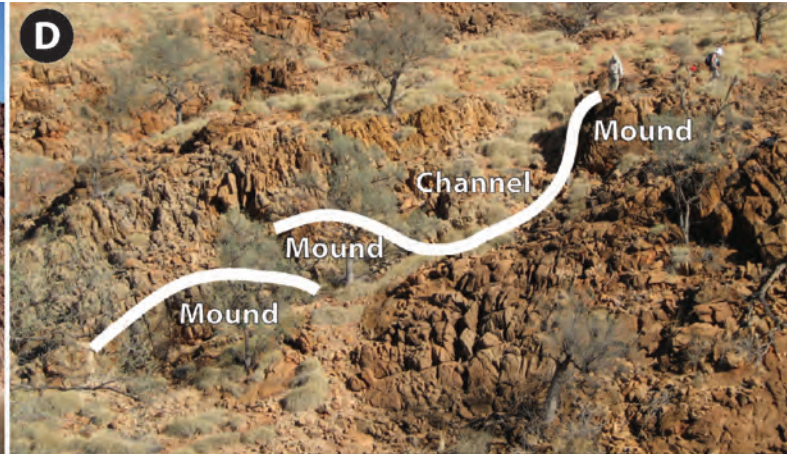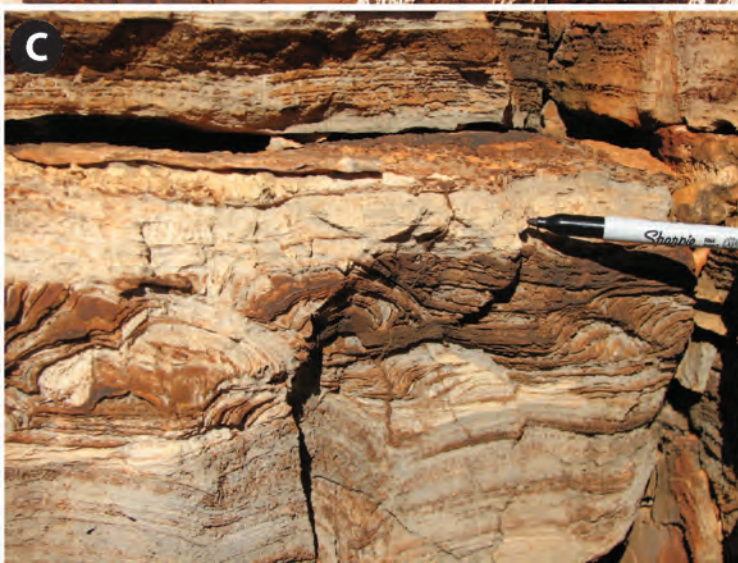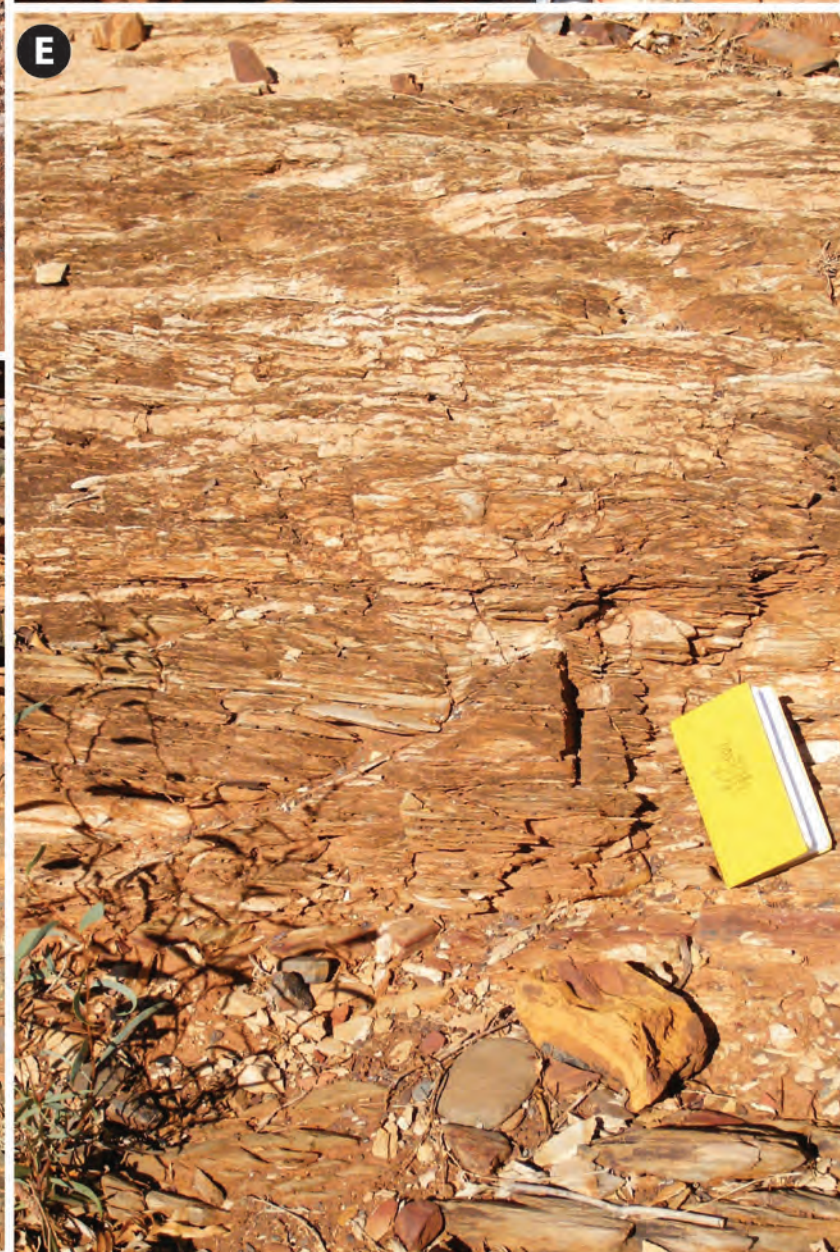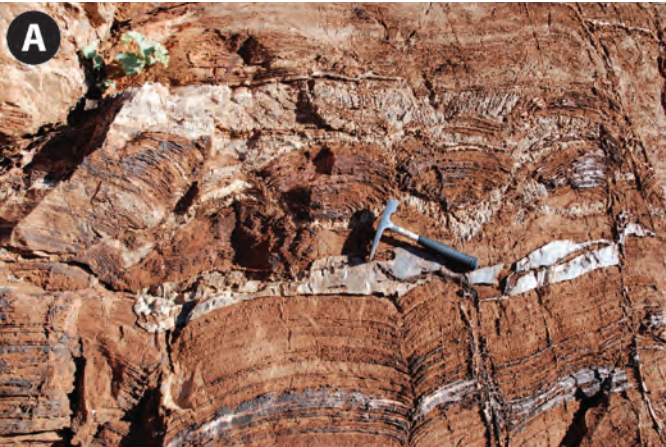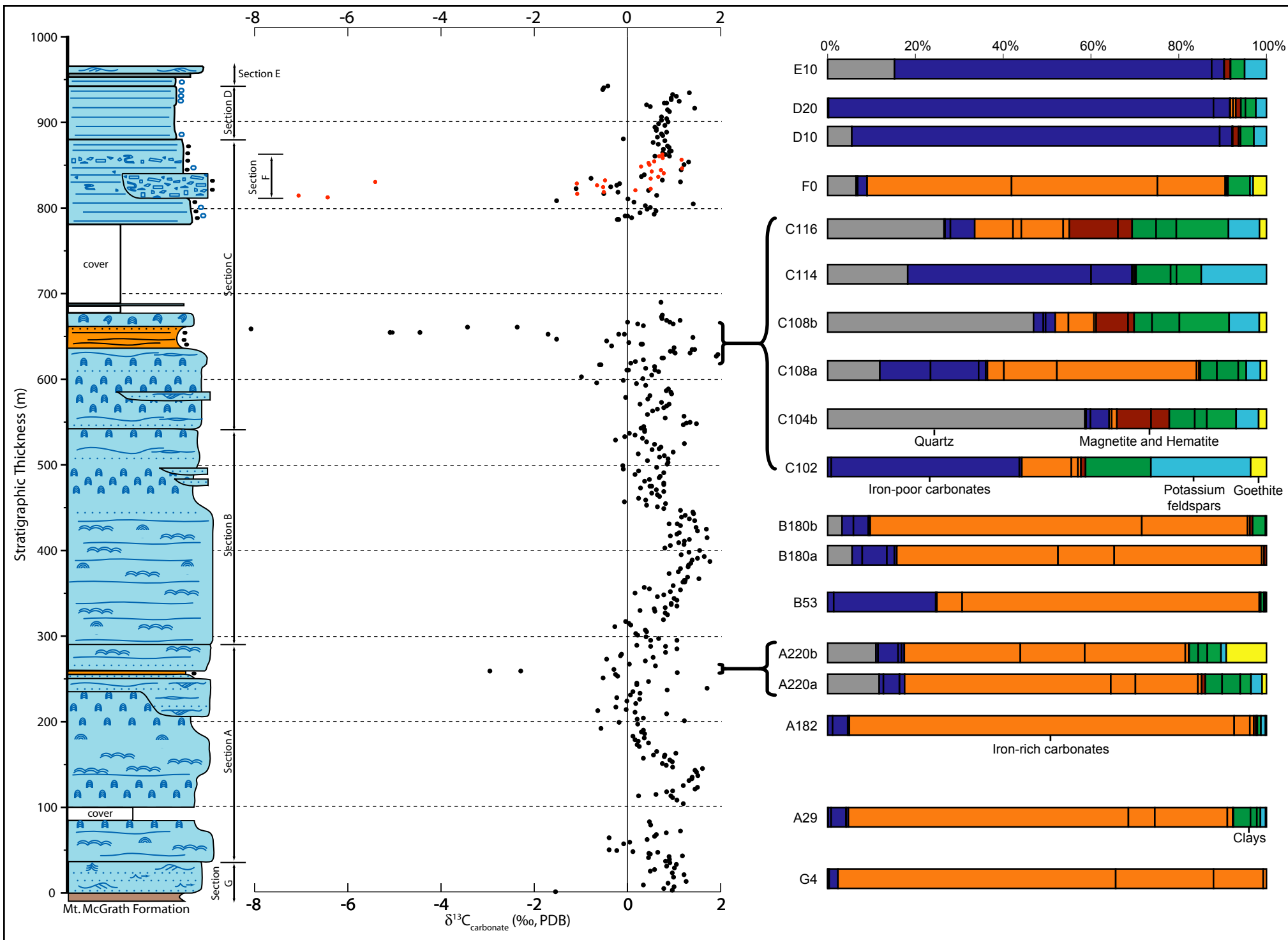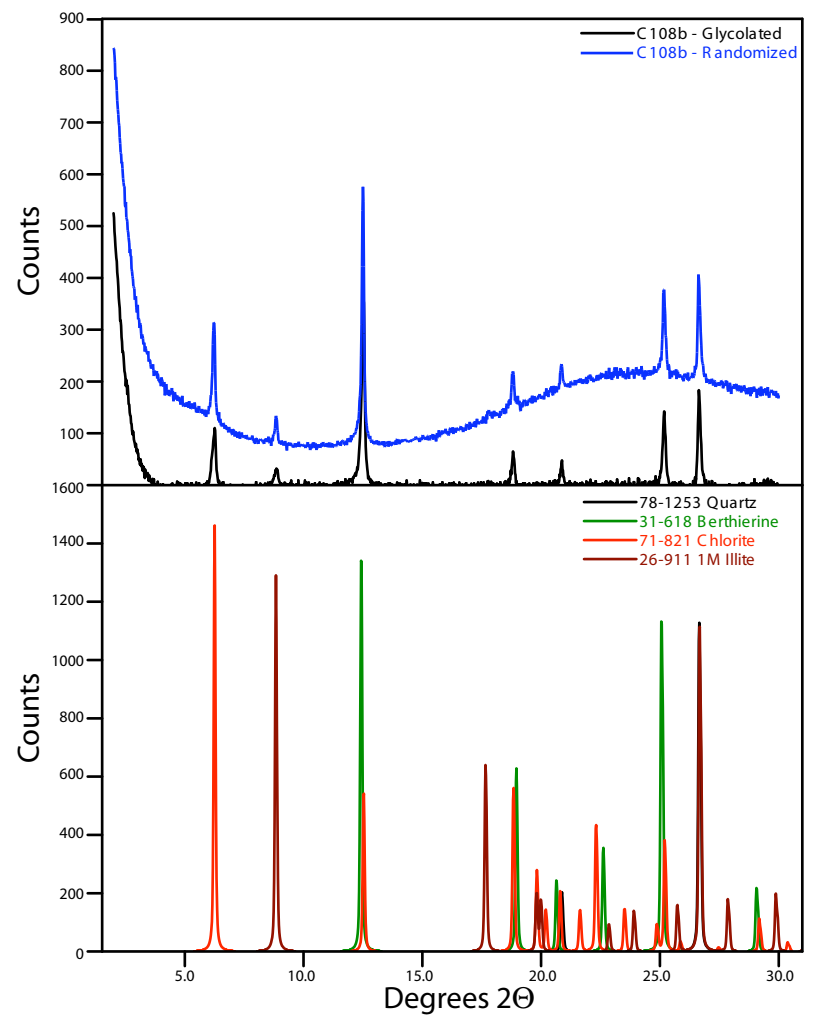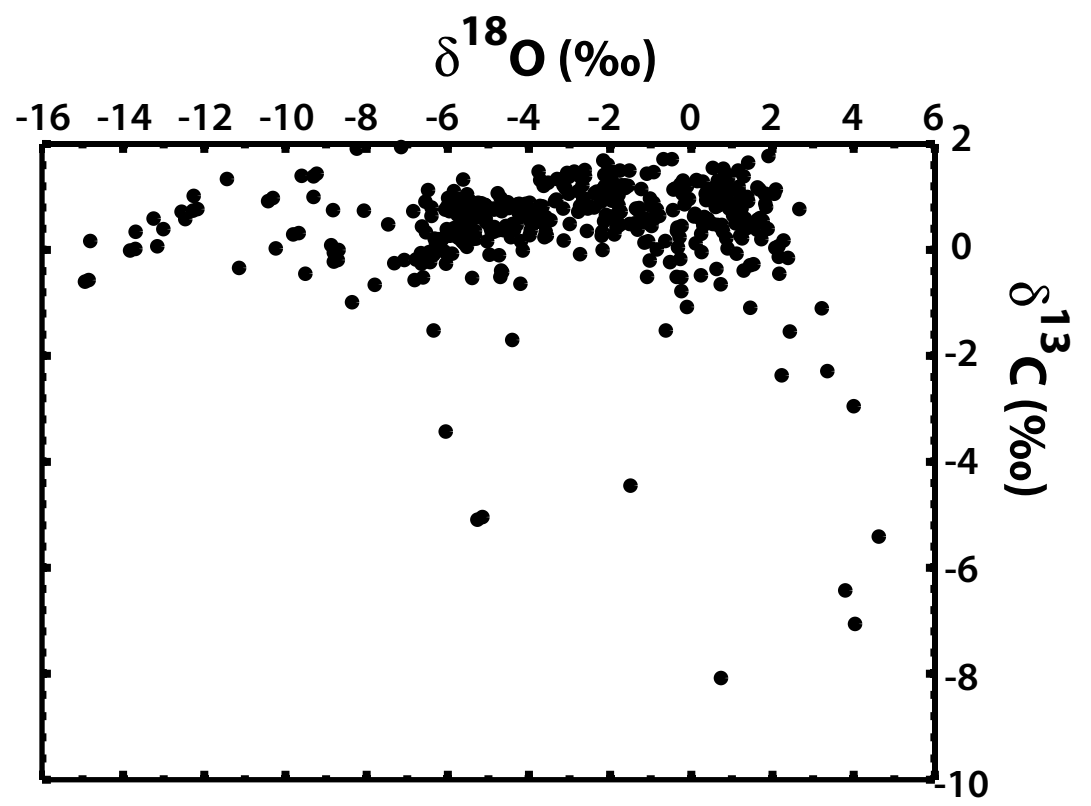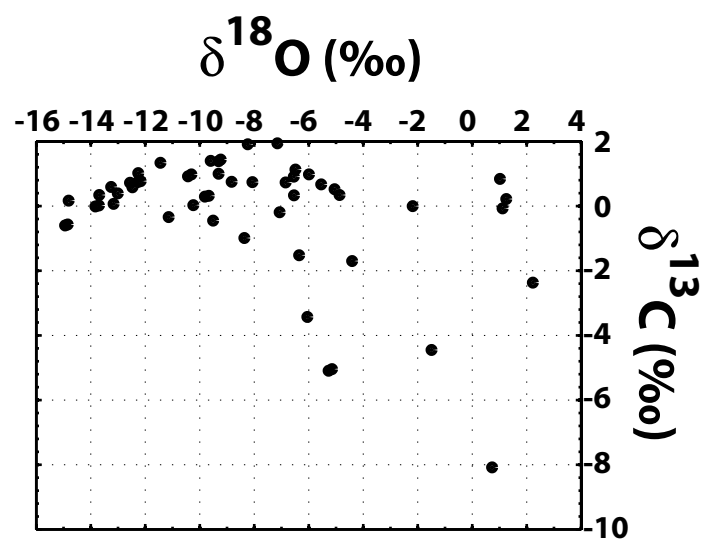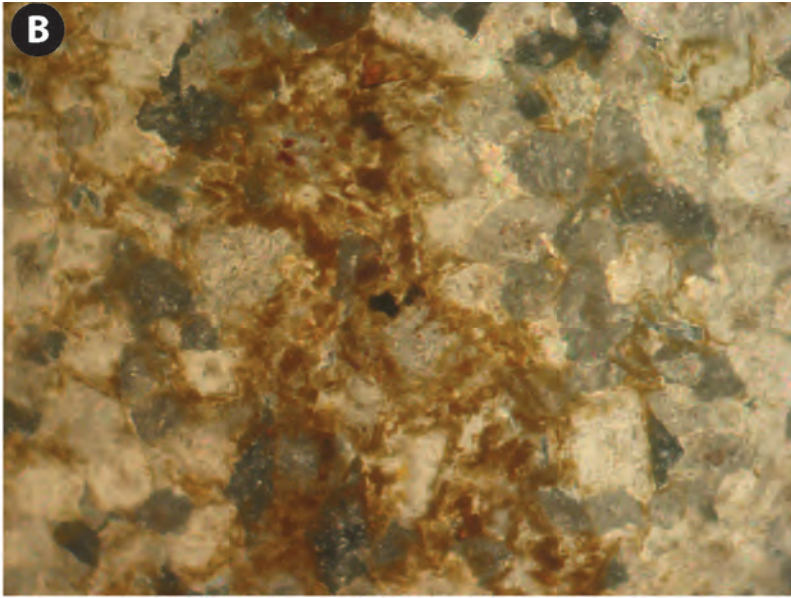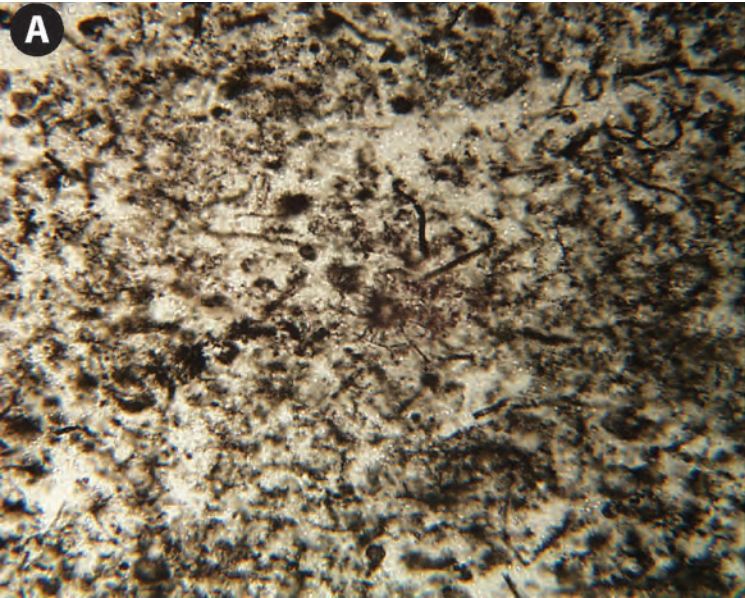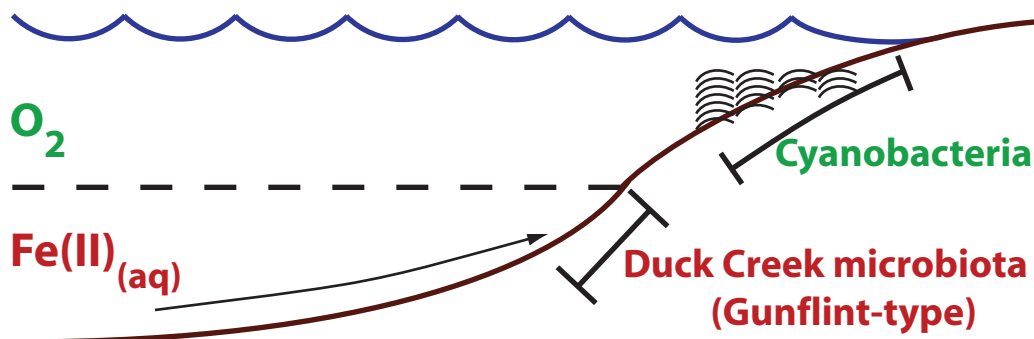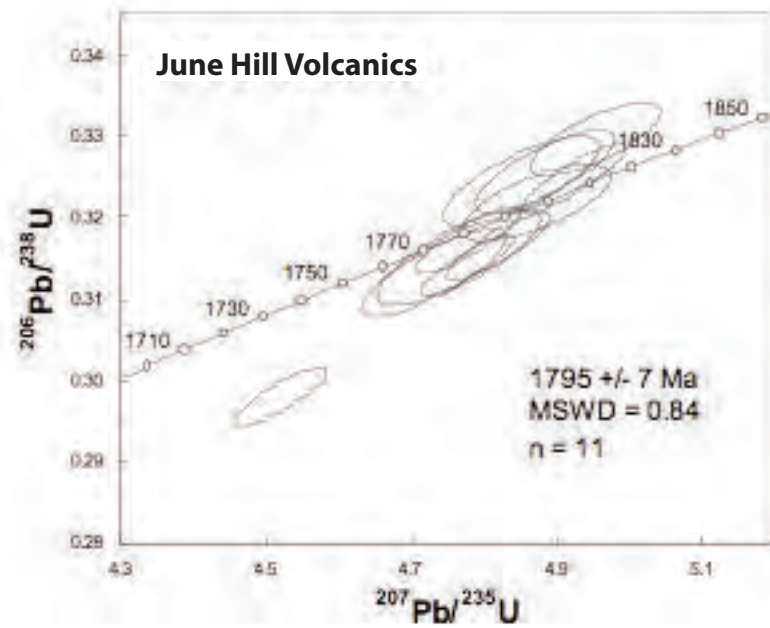
Section	Sample ID	Sample meterage	δ18O final	δ13C final
G	000	000	2.428	-1.54
G	002	002	1.289	0.96
G	004	004	1.238	0.78
G	006	006	1.382	1.00
G	008	008	0.786	0.34
G	010	010	1.821	0.87
G	012	012	0.778	1.26
G	017	017	0.753	0.99
G	020	020	0.604	1.21
G	022	022	-0.059	0.96
G	024	024	0.529	0.49
G	026	026	0.409	0.58
G	028	028	0.465	1.01
G	030	030	0.675	0.84
G	032	032	1.813	1.05
G	034	034	0.849	0.91
G	036	036	0.99	0.82
G	038	038	0.939	0.90
A	002	040	-0.238	0.45
A	003	041	0.924	0.89
A	004	042	1.629	1.18
A	006	044	-2.995	0.49
A	007	045	0.299	0.46
A	008	046	1.029	0.65
A	009	047	0.105	0.12
A	010	048	-6.608	-0.23
A	011	049	-4.688	-0.39
A	018	056	-2.743	-0.08
A	020	058	-0.331	0.05
A	023	061	-0.344	0.42
A	025	063	1.286	-0.39
A	027	065	0.237	0.58
A	029	067	0.32	0.62
A	031	069	-0.991	0.83
A	033	071	2.084	1.14
A	040	078	1.089	0.50
A	044	082	0.75	0.47
A	065	103	0.76	1.20
A	069	107	-0.219	1.06
A	072	110	-1.017	0.97
A	074	112	-0.288	0.24
A	074	112	-1.965	0.93
A	076	114	-1.898	0.61
A	079	117	-1.793	0.84
A	080	118	-2.108	0.97
A	082	120	0.837	1.45
A	084	122	-1.762	1.50
A	086	124	-0.108	1.20
A	092	130	-3.726	1.32
A	094	132	-3.021	1.38
A	096	134	-2.617	1.39

A	098	136	-2.623	1.51
A	102	140	-3.761	1.48
A	104	142	-3.061	1.45
A	106	144	-2.056	1.61
A	108	146	-2.663	0.97
A	110	148	-2.743	0.83
A	112	150	-3.817	0.75
A	114	152	-2.582	0.96
A	116	154	-2.22	0.91
A	118	156	-2.195	0.34
A	120	158	-1.285	0.79
A	122	160	-3.468	0.56
A	122	160	-2.566	0.80
A	124	162	-1.793	1.04
A	126	164	-3.637	0.63
A	132	170	-5.776	0.25
A	134	172	-5.307	0.21
A	136	174	-4.569	0.45
A	138	176	-5.742	0.23
A	140	178	-5.029	0.16
A	142	180	-5.331	0.36
A	144	182	-6.291	0.12
A	147	185	-3.955	0.37
A	149	187	-5.948	0.30
A	151	189	-4.922	0.34
A	153	191	-6.82	-0.57
A	158	196	-5.579	0.22
A	160	198	-6.785	-0.18
A	162	200	-2.68	1.22
A	164	202	-6.321	0.21
A	165	203	-3.588	0.34
A	170	208	-5.07	0.84
A	172	210	-5.507	0.16
A	174	212	-4.211	-0.64
A	175	213	-6.082	-0.03
A	178	216	-7.319	-0.25
A	182	220	-3.142	0.18
A	185	223	-4.153	-0.01
A	187	225	-6.057	0.26
A	189	227	-6.436	-0.23
A	192	230	-5.53	0.06
A	194	232	-2.206	0.27
A	196	234	-5.595	0.12
A	198	236	-4.59	0.85
A	200	238	-0.685	1.71
A	204	242	-6.24	0.20
A	206	244	-5.397	0.20
A	208	246	-5.622	0.45
A	212	250	-6.611	-0.52
A	214	252	-6.505	-0.21
A	216	254	-6.042	-0.26
A	218	256	-4.772	1.07

A	220	258	4	-2.95
A	220	258	3.352	-2.29
A	222	260	1.446	-0.29
A	226	264	1.69	0.60
A	228	266	2.069	0.04
A	232	270	1.615	0.38
A	234	272	2.167	-0.45
A	236	274	1.758	0.55
A	238	276	2.383	-0.15
A	240	278	2.153	-0.13
A	242	280	1.009	0.82
A	246	284	1.83	1.06
A	249	287	1.238	0.82
A	249	287	1.354	0.50
A	250	288	1.726	0.20
B	000	294	1.42	0.50
A	256	294	2.044	1.06
B	002	296	1.09	0.67
B	004	298	1.884	0.40
B	006	300	0.862	0.22
B	008	302	2.27	0.18
B	010	304	1.371	0.41
B	012	306	0.762	0.38
B	016	310	1.531	-0.27
B	018	312	2.148	0.07
B	020	314	0.897	0.03
B	022	316	0.253	-0.04
B	024	318	2.664	0.77
B	030	324	-0.165	0.86
B	032	326	1.839	0.81
B	034	328	1.322	0.59
B	035	329	1.205	0.27
B	037	331	1.635	0.57
B	038	332	0.598	0.81
B	040	334	1.197	1.06
B	042	336	0.897	0.94
B	043	337	0.366	0.94
B	047	341	0.351	1.06
B	049	343	0.784	1.00
B	051	345	-0.793	0.64
B	053	347	0.932	0.78
B	055	349	-1.061	0.16
B	057	351	1.398	0.92
B	059	353	1.682	1.14
B	060	354	0.643	0.47
B	062	356	-2.571	0.36
B	064	358	0.589	0.98
B	068	362	1.17	1.19
B	068	362	0.832	1.23
B	070	364	-1.639	1.22
B	070	364	-0.27	1.24
B	072	366	0.79	1.53

B	074	368	0.283	1.29
B	078	372	-0.934	0.89
B	080	374	0.526	1.09
B	084	378	0.94	1.14
B	086	380	0.144	1.30
B	088	382	0.653	1.31
B	090	384	0.907	1.36
B	092	386	1.899	1.77
B	094	388	1.291	1.39
B	096	390	1.156	1.50
B	098	392	1.4	1.65
B	100	394	0.411	1.15
B	103	397	0.126	1.32
B	105	399	0.53	1.55
B	108	402	-2.396	0.80
B	111	405	-1.831	0.92
B	112	406	-1.561	1.21
B	114	408	-2.335	1.10
B	116	410	-1.723	1.22
B	118	412	-2.047	1.33
B	120	414	-0.48	1.71
B	122	416	-3.363	0.92
B	124	418	-3.019	1.06
B	126	420	-2.788	1.11
B	128	422	-1.525	1.50
B	130	424	-2.17	1.69
B	132	426	-0.927	1.47
B	134	428	-2.084	1.14
B	136	430	-3.984	0.89
B	136	430	-2.383	1.07
B	140	434	-3.039	1.44
B	142	436	-3.215	1.33
B	144	438	-3.098	1.16
B	146	440	-1.89	1.24
B	148	442	-2.144	1.42
B	150	444	-2.762	1.40
B	152	446	-2.19	1.14
B	154	448	-4.139	0.78
B	156	450	-3.953	0.64
B	158	452	-4.944	0.41
B	160	454	-3.662	0.82
B	162	456	-5.895	-0.07
B	164	458	-4.581	0.39
B	166	460	-4.444	0.24
B	168	462	-3.844	0.69
B	170	464	-3.912	0.64
B	172	466	-3.846	0.52
B	174	468	-2.705	0.78
B	176	470	-3.591	0.62
B	178	472	-3.981	0.28
B	180	474	-3.614	0.48
B	180	474	-3.948	0.52

B	182	476	-4.87	0.78
B	184	478	-3.158	0.78
B	186	480	-4.366	0.37
B	188	482	-4.304	0.47
B	190	484	-1.807	0.68
B	192	486	-3.803	0.70
B	194	488	-4.199	0.16
B	196	490	-2.551	0.78
B	198	492	-3.619	0.24
B	200	494	-4.975	-0.09
B	202	496	-1.955	0.63
B	204	498	-4.736	-0.10
B	206	500	-5.085	0.85
B	208	502	-4.242	0.87
B	210	504	-4.478	0.43
B	212	506	-4.079	0.87
B	214	508	-4.248	0.69
B	216	510	-4.497	0.79
B	218	512	-5.393	0.23
B	220	514	-4.699	0.98
B	223	517	-3.786	0.53
B	224	518	-5.164	0.68
B	226	520	-2.786	0.72
B	229	523	-5.061	0.58
B	230	524	-3.154	1.22
B	232	526	-5.845	0.41
B	234	528	-6.648	-0.26
B	236	530	-5.94	0.32
B	238	532	-6.66	-0.06
B	240	534	-5.651	0.16
B	242	536	-6.248	0.04
B	244	538	-4.628	0.37
B	246	540	-4.76	0.37
B	248	542	-6	0.29
B	250	544	-5.592	0.35
C	002	546	-2.134	1.20
C	003	547	-2.883	1.48
C	004	548	-3.528	1.27
C	005	549	-3.31	1.34
C	010	554	-4.082	0.81
C	012	556	-3.642	1.21
C	014	558	-4.853	0.43
C	018	562	-2.149	0.54
C	020	564	-4.181	0.64
C	022	566	-5.384	0.78
C	024	568	-5.896	0.84
C	026	570	-5.252	0.89
C	026	570	-5.948	0.27
C	028	572	-5.962	0.73
C	032	576	-6.637	0.44
C	034	578	-6.46	-0.04
C	036	580	-7.472	0.48

C	038	582	-3.326	0.95
C	040	584	-5.7	0.93
C	042	586	-3.733	0.83
C	044	588	-5.175	0.88
C	048	592	-6.023	0.39
C	050	594	-6.146	0.19
C	051	595	-7.798	-0.66
C	054	598	-6.353	-0.09
C	056	600	-6.54	0.33
C	058	602	-8.362	-0.99
C	060	604	-5.055	0.52
C	064	608	-5.544	0.67
C	**066**	610	**-13.25**	**0.59**
C	**066**	610	**-13.70**	**0.02**
C	**066**	610	**-13.83**	**-0.01**
C	**068**	612	**-13.01**	**0.39**
C	**070**	614	**-12.47**	**0.58**
C	**072**	616	**-14.85**	**-0.57**
C	**072**	616	**-14.94**	**-0.60**
C	**074**	618	**-13.16**	**0.07**
C	**076**	620	**-14.81**	**0.17**
C	**078**	622	**-13.69**	**0.34**
C	**080**	624	**-12.17**	**0.77**
C	**080**	624	**-12.28**	**0.74**
C	**082**	626	**-8.24**	**1.91**
C	**084**	628	**-7.15**	**1.94**
C	**086**	630	**-12.26**	**1.02**
C	**086**	630	**-11.44**	**1.34**
C	**088**	632	**-10.31**	**0.98**
C	**088**	632	**-10.43**	**0.92**
C	**090**	634	**-9.23**	**1.44**
C	**090**	634	**-9.31**	**1.39**
C	**092**	636	**-9.31**	**1.00**
C	**094**	638	**-11.14**	**-0.34**
C	**096**	640	**-9.67**	**0.32**
C	**096**	640	**-9.81**	**0.29**
C	**098**	642	**-10.24**	**0.03**
C	**100**	644	**-9.51**	**-0.45**
C	**102**	646	**-6.35**	**-1.52**
C	**104**	648	**-9.60**	**1.40**
C	108	652	1.114	-0.07
C	**108**	652	**-7.07**	**-0.19**
C	**108**	652	**-4.41**	**-1.70**
C	110	654	-1.496	-4.45
C	**110**	654	**-5.15**	**-5.04**
C	**110**	654	**-5.27**	**-5.09**
C	114	658	0.732	-8.08
C	116	660	2.223	-2.37
C	**116**	660	**-6.05**	**-3.43**
C	**118**	662	**-4.87**	**0.34**
C	120	664	1.249	0.22
C	**120**	664	**-5.99**	**0.98**

C	122	666	-2.186	0.00
C	**122**	**666**	**-6.55**	**0.91**
C	124	668	1.019	0.84
C	**124**	**668**	**-6.49**	**1.13**
C	**126**	**670**	**-8.07**	**0.74**
C	**128**	**672**	**-6.85**	**0.73**
C	**130**	**674**	**-8.83**	**0.75**
C	**145**	**689**	**-12.56**	**0.72**
C	**242**	**786**	**-8.71**	**-0.19**
C	**242**	**786**	**-8.81**	**-0.22**
C	**244**	**788**	**-8.87**	**0.09**
C	**246**	**790**	**-8.69**	**0.00**
C	**246**	**790**	**-8.81**	**-0.05**
C	248	792	0.339	0.57
C	250	794	-3.559	0.27
C	252	796	-0.886	0.61
C	254	798	-1.848	0.42
C	256	800	-1.52	0.49
C	258	802	-1.323	0.38
C	260	804	-1.969	1.41
C	262	806	-1.156	0.14
F	000	808	3.79	-6.43
C	264	808	-0.625	-1.52
F	002	810	4.037	-7.06
C	266	810	-0.851	0.01
F	004	812	-0.109	-1.08
F	006	814	-1.092	-0.51
C	270	814	0.065	0.63
F	008	816	-0.644	0.17
C	272	816	-0.362	-0.51
F	010	818	-1.395	0.50
C	274	818	-1.024	-0.20
F	012	820	-0.241	-0.52
C	276	820	-0.982	0.45
F	014	822	0.725	-0.65
C	278	822	3.216	-1.10
F	016	824	1.449	-1.09
C	280	824	0.624	-0.36
F	018	826	4.622	-5.41
C	282	826	-0.525	-0.23
F	020	828	0.237	-0.48
C	284	828	-0.273	-0.17
F	022	830	-1.036	0.50
C	286	830	-0.443	1.14
F	024	832	-2.101	0.66
C	288	832	-0.452	0.75
C	290	834	-0.244	-0.78
F	028	836	-1.366	0.78
C	292	836	0.247	0.30
F	030	838	-1.126	0.52
C	294	838	-0.357	0.36
F	032	840	-1.741	0.72

F	034	842	-1.627	1.17
F	036	844	-1.9	0.29
C	300	844	-1.233	1.15
F	038	846	-1.767	0.47
F	040	848	-1.374	0.45
F	042	850	-1.161	0.57
C	306	850	-1.869	1.21
F	044	852	-0.396	1.16
C	309	853	-0.205	1.31
F	046	854	-0.85	0.76
F	048	856	0.091	0.68
F	050	858	-1.31	0.75
D	000	860	-5.789	0.90
C	316	860	-1.139	0.59
D	002	862	-6.01	0.82
D	004	864	-6.067	0.76
D	005	865	-5.415	0.90
D	006	866	-5.653	0.94
D	008	868	-5.97	0.77
D	010	870	-5.826	0.89
D	012	872	-5.757	0.86
D	014	874	-5.762	0.66
D	016	876	-5.437	0.55
D	018	878	-6.404	0.80
D	020	880	-6.455	-0.09
D	022	882	-6.403	0.64
D	024	884	-4.858	0.76
D	026	886	-5.284	0.73
D	028	888	-5.459	0.84
D	030	890	-5.263	0.62
D	032	892	-5.213	0.62
D	034	894	-5.455	0.59
D	036	896	-5.094	0.80
D	038	898	-5.285	0.67
D	040	900	-4.623	0.87
D	042	902	-5.263	0.73
D	044	904	-5.218	0.84
D	046	906	-4.672	0.73
D	052	912	-4.524	0.90
D	054	914	-4.283	0.86
D	056	916	-1.1	1.44
D	058	918	-4.405	0.49
D	060	920	-4.494	0.41
E	000	922	-5.572	0.84
D	062	922	-4.672	0.79
E	002	924	-5.847	1.11
E	004	926	-5.765	0.94
E	006	928	-5.764	0.94
E	008	930	-5.528	1.05
E	010	932	-5.502	0.97
E	012	934	-5.621	1.33
E	016	938	-5.398	-0.53

| E | 018 | 940 | -4.704 | -0.51 |
| E | 020 | 942 | -4.662 | -0.42 |

Sample Name	#	Quartz	Calcite	Mg-calcite	Aragonite	Dolomite	Fe-Dolomite	Ankerite	Magnesite	Siderite	Halite	Pyrite	Anhydrite	Magnetite	Hematite	Goethite
E10	18	15.2	71.9	2.8	0.0	0.0	0.0	0.0	0.0	0.0	0.2	0.0	0.1	0.0	1.4	0.0
D20	17	0.2	85.6	3.6	0.0	0.6	0.0	0.6	0.1	0.0	0.2	0.0	0.0	0.0	1.1	0.0
D10	16	5.4	82.7	2.8	0.0	0.0	0.0	0.1	0.0	0.0	0.2	0.0	0.1	0.0	1.3	0.0
F0	15	6.4	0.4	2.1	0.0	32.5	32.8	15.3	0.0	0.3	0.3	0.1	0.0	0.0	0.3	3.0
C116	14	25.3	0.2	1.2	0.0	8.3	1.8	9.1	5.3	1.3	0.2	0.0	0.2	3.1	10.6	1.5
C114	13	17.8	40.8	9.1	0.0	0.2	0.0	0.4	0.1	0.0	0.1	0.1	0.1	0.1	0.1	0.0
C108b	12	45.5	2.2	0.5	0.0	2.9	0.0	5.7	2.1	0.5	0.2	0.0	0.1	1.3	7.1	1.6
C108a	11	11.7	11.4	10.8	1.6	3.7	11.9	31.5	0.4	0.6	0.2	0.2	0.0	0.0	0.3	1.4
C104b	10	53.6	0.3	0.0	0.9	0.5	0.0	0.0	3.9	1.1	0.1	0.0	0.4	3.8	7.2	1.6
C102	9	0.0	0.8	42.0	0.0	11.1	0.0	1.4	0.6	0.7	0.6	0.1	1.4	1.0	0.0	3.5
B180b	8	3.2	2.6	3.3	0.2	60.7	0.0	23.6	0.2	0.5	0.4	0.1	0.0	0.0	0.6	0.0
B180a	7	5.5	2.3	5.6	1.7	36.7	12.8	33.6	0.6	0.5	0.0	0.2	0.0	0.0	0.5	0.0
B53	6	0.0	1.4	23.0	0.0	0.0	5.7	67.0	0.3	0.1	0.2	0.0	0.0	0.0	0.2	0.3
A220b	5	10.8	0.5	4.5	0.8	25.9	14.4	22.5	0.6	0.8	0.6	0.3	0.0	0.0	0.1	9.0
A220a	4	11.3	0.9	3.5	0.0	45.2	5.4	13.7	1.1	0.8	0.5	0.2	0.0	0.0	0.8	1.0
A182	3	0.0	1.1	3.4	0.3	86.5	0.0	3.5	0.1	0.9	0.9	0.0	0.0	0.0	0.5	0.2
A29	2	0.1	0.7	3.3	0.0	62.3	5.9	16.1	0.5	1.2	1.2	0.2	0.0	0.0	0.2	0.2
G4	1	0.0	0.3	2.0	0.0	62.7	22.1	11.2	0.0	0.7	0.9	0.0	0.0	0.0	0.0	0.0

Anatase	Rutile	ordered Microcline feldspar	intermediate Microcline feldspar	Sanidine feldspar	Orthoclase feldspar	Oligoclase feldspar (North Carolina)	Total non-clays	Na-Smectite (Wyo)	Ca-smectite (Wyo)	1Md illite (+ dioct mica & smectite)
0.0	0.2	0.0	0.1	0.5	0.0	4.3	96.8			
0.0	0.2	0.4	0.3	0.0	0.3	1.4	94.6			
0.1	0.2	0.1	0.1	0.5	0.5	1.6	95.8			1.0
0.0	0.0	0.0	0.0	0.0	0.0	0.7	94.0			1.6
0.0	0.0	0.8	1.8	2.5	0.4	1.2	74.8			0.0
0.0	0.0	0.0	2.0	7.6	4.7	0.3	83.4			0.3
0.0	0.0	0.2	3.0	2.7	0.5	0.2	76.2			1.7
0.0	0.0	0.0	0.8	1.2	0.8	0.5	89.0			0.8
0.0	0.0	0.0	2.3	0.5	0.4	1.6	78.1			
0.0	0.0	0.0	7.8	3.5	8.5	2.4	85.4			
0.0	0.0	0.0	0.0	0.0	0.0	0.2	95.6			1.1
0.0	0.0	0.0	0.0	0.0	0.0	0.0	100.0			
0.0	0.0	0.0	0.0	0.1	0.2	0.0	98.6			0.7
0.0	0.0	0.1	0.1	0.0	0.5	0.5	91.8			2.8
0.0	0.0	0.3	1.2	0.0	0.0	0.9	86.8			2.4
0.0	0.0	0.0	0.0	0.4	0.0	0.6	98.5			
0.0	0.0	0.0	0.0	0.7	0.0	0.5	93.0			0.8
0.0	0.0	0.0	0.0	0.0	0.0	0.0	100.0			

1M Illite (R>2; 88%I)	1M illite (R>1, 70-80%I)	Glauconite	Biotite (2M1)	Berthierine	Muscovite (2M1)	Illite (1M, PD3B)	Montmorillonite (Webster Pass)	Chlorite	Fe-chlorite	Total clays	Total detrital component	Other clays	Stratigraphic height in meters
1.4								1.8		3.2	4.9	3.2	932
		1.0						2.3		3.3	2.4	2.3	880
		0.4	0.0				0.7	1.3		3.5	2.8	3.0	870
	0.0				3.1			0.2		4.9	0.7	4.9	808
6.3		5.2		4.4		0.6	0.4	4.0		20.9	6.7	11.3	660
		7.7		1.3	3.7		1.5			14.5	14.5	5.5	658
		4.0		6.1				6.3	2.9	21.0	6.7	11.0	652
		3.7		4.8				1.0		10.3	3.2	1.8	652
1.4		5.3		2.5			1.2	3.5		13.9	4.7	6.1	648
				14.6						14.6	22.3	0.0	646
				0.0				1.7		2.9	0.2	2.9	474
										0.0	0.0	0.0	474
										0.7	0.3	0.7	347
		2.0		2.0				0.3		7.1	1.2	3.1	258
		3.7		4.0						10.0	2.4	2.4	258
0.6		0.1		0.2				0.2		1.1	1.0	0.8	220
		3.8		1.4						6.0	1.2	0.8	67
										0.0	0.0	0.0	4

Table 3: SHRIMP isotopic data for zircons from the June Hill Tuff (Mount 09-20B).

Grain-spot	U (ppm)	Th (ppm)	232Th /238U	% common 206Pb	207Pb /206Pb	+/-1σ	207Pb /235U	+/-1σ	206Pb /238U	+/-1σ	207Pb /206Pb Age (Ma)	+/-1σ	Conc. (%)
Magmatic population													
1-Aug	362	87	0.25	0	0.1104	0.0005	4.82	0.05	0.317	0.003	1806	9	102
2-Aug	564	208	0.38	0.07	0.1102	0.0005	4.77	0.04	0.314	0.002	1803	7	102
1-Nov	673	442	0.68	0.22	0.1099	0.0005	4.52	0.04	0.298	0.002	1799	9	107
28-1	405	77	0.2	0.01	0.1098	0.0005	4.92	0.05	0.325	0.003	1797	8	99
23-1	231	52	0.23	0.02	0.1097	0.0011	4.87	0.07	0.322	0.003	1795	18	100
18-1	119	43	0.37	0.18	0.1096	0.001	4.76	0.07	0.315	0.004	1793	17	101
30-1	151	45	0.3	0.04	0.1095	0.0009	4.73	0.07	0.313	0.004	1790	15	102
1-Oct	422	125	0.3	0.08	0.1092	0.0006	4.78	0.05	0.317	0.003	1785	10	100
17-1	322	56	0.18	0.34	0.1089	0.0009	4.95	0.06	0.33	0.003	1781	14	97
20-1	198	182	0.95	0.12	0.1087	0.0009	4.88	0.06	0.326	0.003	1777	15	98
1-Sep	146	39	0.28	0.11	0.1083	0.001	4.85	0.07	0.325	0.004	1772	17	98
Older zircons													
1-Jul	272	333	1.27	0	0.3	0.0008	29.25	0.28	0.707	0.006	3470	4	101
27-1	82	93	1.17	0.17	0.1817	0.0015	12.86	0.2	0.513	0.007	2668	13	100
1-Mar	286	120	0.43	0.27	0.181	0.0008	12.77	0.13	0.512	0.005	2662	8	100
14-1#	787	447	0.59	0.35	0.1742	0.0007	8.38	0.07	0.349	0.003	2599	7	135
26-1	96	22	0.24	0.31	0.1202	0.0016	5.93	0.11	0.358	0.005	1959	24	99
21-1	138	52	0.39	0.04	0.1121	0.0009	5.04	0.07	0.326	0.004	1834	15	101
Younger zircons													
1-Jun	137	145	1.09	0.08	0.108	0.0008	4.77	0.07	0.32	0.004	1765	14	98
19-1	152	75	0.51	0.12	0.1078	0.0008	4.8	0.06	0.323	0.004	1762	13	98
24-1	104	95	0.94	0.2	0.1066	0.0012	4.54	0.08	0.309	0.004	1742	21	100
1-May	468	452	1	0.3	0.1022	0.0007	4.15	0.04	0.295	0.002	1665	12	100
25-1	125	135	1.11	0.15	0.1006	0.0009	4.11	0.06	0.296	0.004	1635	17	98
1-Dec	60	86	1.47	0.12	0.0984	0.002	3.86	0.1	0.284	0.004	1595	38	99
22-1	157	122	0.8	0.09	0.0967	0.001	3.7	0.07	0.278	0.004	1562	19	99
13-1#	423	266	0.65	0.72	0.0823	0.002	2.2	0.07	0.194	0.004	1252	48	110
29-1	62	84	1.41	0.21	0.0795	0.0025	2.15	0.08	0.197	0.003	1185	63	102

Pb isotopic ratios are for radiogenic Pb after correction for common Pb (204-correction of Compston et al., 1984)

Conc. = concordance.

Reproducibility of U/Pb for BR266 zircon standard was +/-1.31% (2σ; n = 15).

discordance ≥10%: not considered in discussion of age data.